TURKISH COMPUTATIONAL and THEORETICAL CHEMISTRY

In memory of Prof. Dr. Cemil ÖĞRETİR...

15 JUNE 2017 VOLUME: 1 ISSUE: 1

OBITUARY

PROF. DR. CEMİL ÖĞRETİR

(1947–2011)

Prof. Dr. Cemil Öğretir passed away in Eskisehir in 2011. He was a well-known figure who inspired and guided many young academicians, administrators and researchers in the field of chemistry.

Prof. Öğretir was born in Şumnu, Bulgaria in 1947. He completed his primary and high schools in Eskisehir. After completing his high school education in 1964, he became a student in the Chemistry Department of Middle East Technical University with a scholarship from TUBITAK and graduated in 1970. He also obtained bursary from Turkish Ministry of Education and completed his MSc and PhD studies under Prof.Dr.A.R.Katritzkys supervision in East Anglia University, England in 1972 and 1975, respectively. He was also honored with a post-doc position by the same university in 1976. After completing his post-doc researches on "Synthesis and addition reactions of betains" he returned to Turkey and started to work as an Assistant Doctor in the Academy of Eskisehir Engineering and Architecture in 1976. He became Associate Professor and full Professor in 1979 and 1987, respectively. He was then appointed as the first chairman of the Chemistry Department of Anadolu University just after Engineering and Architecture Academy joined to Anadolu University in 1981. He continued to work at the same department until 1993 when he moved to the newly established Eskişehir Osmangazi University. He worked as the chairman of the Chemistry Department of Eskişehir Osmangazi University between 1996 and 2002. In addition to his mentioned activities during 1976 and 2010, he played very important roles in the establishment and development of his university as being head of various departments, manager of Science Research Center, head of the Department of Foreign Languages, member in various academic committees and organizations.

He has given various lectures based on organic, physical and general chemistry in both undergraduate and graduate levels. He supervised 16 PhD and 34 MSc theses in both Anadolu and Eskişehir Osmangazi Universities on various aspects of organic chemistry. His PhD students became faculty members or academicians in different Universities in Turkey. They include Şeref Demirayak, Ayşe Eren Pütün, Nevin Kanışkan, Mehmet Cebe, Fatma Severcan, Halil Berber, Selma Yarlıgan, Sevgül

Çalış, Müjgan Özkütük, Funda Tay, Murat Duran, Kamuran Görgün, Serife Okur, Ü.Gülşah Koyuncu and Süreyya Hancı. He was among the few scientists who introduced the subject of organic chemistry and computational chemistry, a newly developing field in Turkey, into the research and education programs of universities. He fluently spoke English besides his mother language, Turkish. He published more than 80 scientific papers and several books in the fields of organic and theoretical chemistry. He had two sons and one grandchild.

He was an often adored educator with a warm personality. His students and colleagues reminisce the anecdotes where he always tried to establish strong social ties among the colleagues. Lunches, dinners, tea parties and similar occasions served as stimulators for this purpose. As a mentor, he was keenly interested in the career developments of his students.

With Prof. Öğretir's death, Turkish Chemistry Community has lost a profoundly educated scientist who had an acute sense of responsibility and commitment. His colleagues, friends and students will remember his amiability, strong will and how he positively influenced other academicians with his successful academic career.

Written by

Prof. Dr. Vural Bütün
Eskisehir Osmangazi University,
Dean of Faculty of Science and Letters.

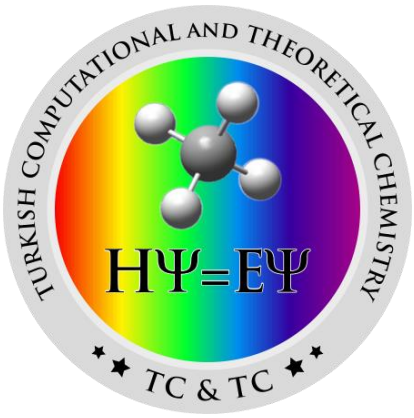

CONTENTS

Turkish Computational and Theoretical Chemistry

Turkish Comp Theo Chem (TC&TC)

Volume(Issue): 1(1) – Year: 2017 – Pages: 1-10

Received: 03.03.2017 ***Accepted:*** 17.03.2017 *Research Article*

Theoretical investigation on electrophilicity indexes and proton affinities of some boron-nitrogen open-chain species

Duran KARAKAŞ[1]

Cumhuriyet University, Science Faculty, Chemistry Department, 58140 Sivas / Turkey

Abstract: Some neutral boron-nitrogen open-chain compounds were optimized at Hartree-Fock (HF) methods with cc-pvdz basis set in the gas phase. Atomic charges were determined by the natural bond orbital (NBO) analysis. HOMO composition was calculated from the atomic orbital coefficients. The compounds were protonated from the atom supplying the highest contribution to HOMO and deprotonated from the most positive charged atom. Electrophilicity indexes of all the species were determined from the optimized structures. A parabolic curve was obtained from the graph of nucleophilicity parameters against electrophilicity indexes of all the chemical species. Electrophilicity indexes of the cationic species were found to be higher than the neutral and anionic species. Electrophilicity indexes increased with increasing of boron/nitrogen ratio for the neutral and cationic species and decreased with increasing of boron/nitrogen ratio for the anionic species. Proton affinities of the neutral and anionic species were calculated to determine their basicities. Proton affinities of the neutral species increased with decreasing of electrophilicity and boron/nitrogen ratio. Whereas proton affinities of the anionic species increased with increasing of electrophilicity.

Keywords: *Theoretical study, Electrophilicity index, Proton affinity, Boron-nitrogen open-chain species*

1. Introduction

Recently, the boron-nitrogen compounds have drawn the attention of scientist due to their promising future in many applications, such as in the field of conducting polymers, the chemical vapor deposition, the fuel cell and the hydrogen storage [1]. The electrophilicity and nucleophilicity are important parameters in the understanding of molecular properties. Quantum chemical calculations have introduced two new important concepts in chemistry. These concepts are chemical potential (μ) [2] and chemical hardness (η) [3]. These quantities are used to predict the acidity and reactivity of chemical species. The definition of these concepts is

$$\mu = -\frac{I + A}{2} \quad (1)$$

$$\eta = \frac{I - A}{2} \quad (2)$$

where I is the ionization potential and A is the electron affinity. (I+A)/2 is the Mulliken electronegativity (χ) for chemical species [2]. Softness (σ) is the inverse of the hardness. According to Koopman's theorem [4,5], I and A depend on frontier molecular orbital energies.

$$I = -E_{HOMO} \quad (3)$$

$$A = -E_{LUMO} \quad (4)$$

[1] Corresponding Author

e-mail: dkarakas@cumhuriyet.edu.tr

Although Pearson's chemical hardness definition is $\eta=(E_{LUMO}–E_{HOMO})/2$, recently, Pearson has used to eq. (5) for calculation of the chemical hardness [6].

$$\eta = E_{LUMO} - E_{HOMO} \quad (5)$$

One way of predicting the interaction between chemical species is to take into consideration of electrophilicity indexes (ω). Parr et al. have defined the electrophilicity index as a measure of energy lowering due to maximal electron flow between donor and acceptor [7]. Electrophilicity index depending on the chemical hardness and chemical potential is given as follows.

$$\omega = \frac{\mu^2}{2\eta} \quad (6)$$

Kiyooka et al. have detected that the ω is a function of μ/η in the second-order parabola for various neutral, cationic and anionic species [8] and they have proposed the ε parameter related to nucleophilicity.

$$\varepsilon = \mu\eta \quad (7)$$

Proton affinity (PA) is very important thermodynamic parameter for determination of gas phase acidities of organic and inorganic compounds. Lewis proposed a definition of acid-base behavior in terms of electron-pair donation and acceptance [9]. According to Lewis definition, electron-pair donation species are considered as Lewis bases and electron-pair acceptances are regarded as Lewis acids. The boron-nitrogen open-chain compounds can be considered as both Lewis acid and Lewis base. Because these compounds have LUMO on the boron atom and HOMO on the nitrogen atom. Acid or base behaviors of these compounds can be determined by calculating PA values. PA can be computed from the energy differences between the interested molecule and the same molecule with one additional proton.

In this study, ω and ε values were calculated for the compounds (H_2BNH_2, H_2BNHBH_2, H_2NBHNH_2, $H_2BNHBHNH_2$, $H_2BNHBHNHBH_2$, $H_2NBHNHBHNH_2$), their geometric isomers, their cationic and anionic species. The ε-ω and boron/nitrogen ratio-ω correlations were investigated for all the species. PA values were obtained for neutral and anionic boron-nitrogen species. The PA-ω and PA-boron/nitrogen ratio relations were determined for the neutral and anionic species.

2. Computational Method

The structures of neutral boron-nitrogen open-chain compounds were drawn in Gaussview 5.0.8 [10]. Geometry optimizations and frequency calculations were made in the gas phase by using Gaussian 09 Revision-A.02 [11]. HF theory [12], density functional theory (DFT) [13], Becke-style three-parameter functional with Lee-Yang-Parr exchange-correlation functional (B3LYP) method [14] and second order Møller-Plesset perturbation (MP2) method [15,16] were used to optimize the structure of the neutral boron-nitrogen open-chain compounds. Dunning's correlation consistent polarized valance double zeta (cc-pvdz) basis set [17-19] was used to represent the atomic orbitals of boron, nitrogen and hydrogen. Geometry optimizations were followed by frequency calculations and no imaginary frequency was found for restricted spin neutral boron-nitrogen compound [20]. The same procedures were applied for the cationic and anionic boron-nitrogen species. Frontier molecular orbital energies (E_{HOMO} and E_{LUMO}) were obtained from HF, B3LYP and MP2 methods with cc-pvdz basis set. But HF molecular orbital theory provides more reliable data on molecular orbital energy levels than DFT method [8]. Therefore, HF results were used to calculate the ω, ε and PA values. The results of DFT and MP2 methods were given in supplementary data.

3. Results and Discussion

3.1 Electronic structures

The electronic structures of some neutral, cationic and anionic boron-nitrogen compounds and their isomers were optimized at HF, B3LYP and MP2 methods with cc-pvdz basis set. The optimized structures at HF/cc-pvdz level of the neutral species and atomic numbering scheme were given in Fig. 1. BH_2NH_2, BH_2NHBH_2 and NH_2BHNH_2 molecules were labeled as **1a**, **2a** and **3a**, respectively. The molecules labeling with **4a-4b, 5a-5c** and **6a-6c** are the geometric isomers of $NH_2BHNHBH_2$, $NH_2BHNHBHNH_2$ and $BH_2NHBHNHBH_2$, respectively. All the molecules are almost planar. Both nitrogen and boron atoms have sp^2 hybridization in all neutral molecules. The

molecular structures support sp^2 hybridization. Nitrogen atoms p orbitals which is perpendicular to the plane of the molecule form π-bonds between boron and nitrogen atoms.

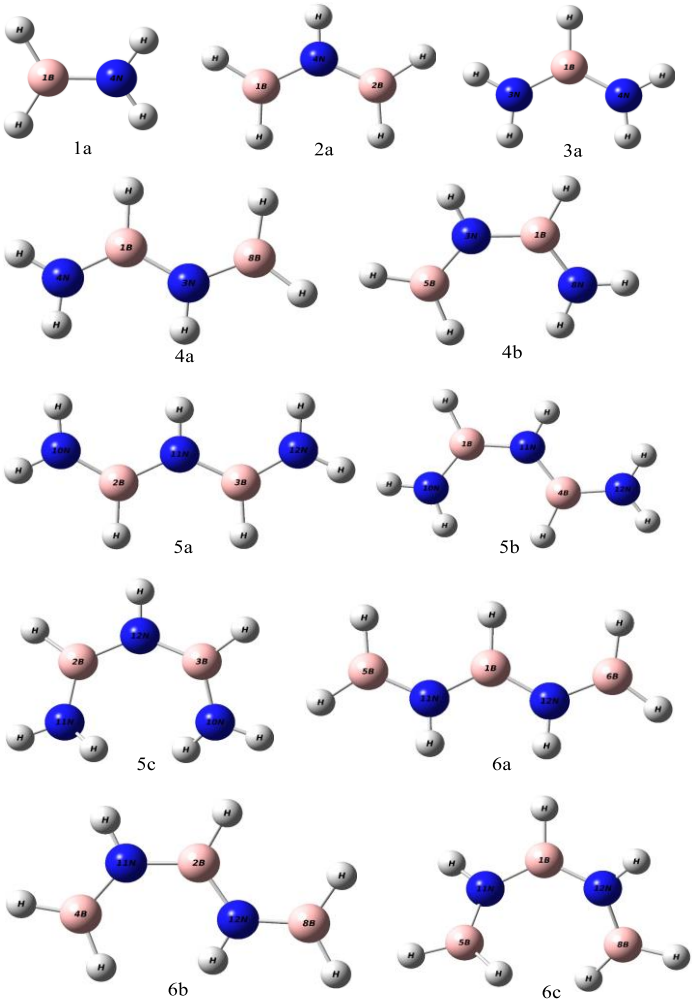

Fig. 1. Molecular structures of some neutral boron-nitrogen compounds optimized at HF/cc-pvdz level and atomic numbering scheme.

3.2 Protonation and deprotonation

The neutral species coordinate with proton by giving HOMO electrons. Therefore, HOMO composition was taken into account for protonation of the neutral species. The compounds given in Fig. 1 were protonated from the atom supplying the highest contribution to HOMO. HOMO composition of boron and nitrogen atoms were calculated from eq. (8) [21] and given in Table 1.

$$\%\,HOMO\ composition = \frac{n^2}{\sum n^2} x100 \qquad (8)$$

where n is the coefficients of atomic orbitals for a certain atom in a molecule and $\sum n^2$ is the sum of the squares of all atomic orbital coefficients in a specific molecular orbital.

Table 1. % HOMO composition of boron and nitrogen atoms calculated at HF/cc-pvdz level

Molecules	% HOMO composition
1a	8.5(1B), 91.5(4N)
2a	5.0(1B), 5.0(2B), 90.0(4N)
3a	0.4(1B), 49.8(3N), 49.8(4N)
4a	1.0(1B), 37.2(3N), 57.7(4N), 4.1(8B)
4b	1.2(1B), 35.7(3N), 1.2(5B), 59.4(8N)
5a	0.3(2B), 0.3(3B), 29.1(10N), 41.2(11N), 29.1(12N)
5b	0.3(1B), 0.3(4B), 32.1(10N), 42.0(11N), 25.2(12N)
5c	1.2(2B), 1.2(3B), 25.9(10N), 26.0(11N), 45.7(12N)
6a	0.4(1B), 4.3(5B), 4.3(6B), 45.5(11N), 45.5(12N)
6b	0.4(2B), 3.8(4B), 4.6(8B), 43.2(11N), 47.9(12N)
6c	2.8(1B), 4.3(5B), 4.3(8B), 44.2(11N), 44.3(12N)

NBO atomic charges were considered to remove the proton from the neutral species. The more positive charged atom is the more electron-withdrawing from X-H (X=B or N) bond. Therefore, separation of H^+ from the positive charged atom is easier than the negative charged atom. NBO charges of boron and nitrogen atoms were calculated at HF/cc-pvdz level for deprotonation. NBO charges were given in Table 2.

Table 2. NBO charges of boron and nitrogen atoms calculated at HF/cc-pvdz level

Molecules	NBO charges
1a	0.601(1B), -1.111(4N)
2a	0.679(1B), 0.679(2B), -1.227(4N)
3a	0.919(1B), -1.154(3N), -1.154(4N)
4a	0.957(1B), -1.226(3N), -1.142(4N), 0.648(8B)
4b	0.956(1B), -1.233(3N), 0.650(5B), -1.141(8N)
5a	0.949(2B), 0.949(3B), -1.147(10N), -1.144(11N), -1.147(12N)
5b	0.948(1B), 0.951(4B), -1.147(10N), -1.250(11N), -1.144(12N)
5c	0.950(2B), 0.950(3B), -1.155(10N), -1.155(11N), -1.259(12N)
6a	1.007(1B), 0.663(5B), 0.663(6B), -1.231(11N), -1.231(12N)
6b	1.010(2B), 0.661(4B), 0.661(8B), -1.236(11N), -1.234(12N)
6c	1.026(1B), 0.663(5B), 0.664(8B), -1.241(11N), -1.241(12N)

3.3 Electrophilicity indexes

HOMO and LUMO energies of the cationic, neutral and anionic boron-nitrogen compounds were obtained from the optimized structure at HF/cc-pvdz level of theory. μ, η, ε and ω were calculated from eq. (1), (5), (6) and (7), respectively. These values were given in Table 3.

As can be seen from Table 3, HOMO and LUMO energy rankings for a certain compound are in the form cationic < neutral < anionic. For example, HOMO and LUMO energy diagrams of $H_2BNH_3^+$, H_2BNH_2 and $HBNH_2^-$ species were given in Fig. 2. The cationic species have lower HOMO and LUMO energy levels than the neutral and anionic species. There is almost the same tendency in the other species.

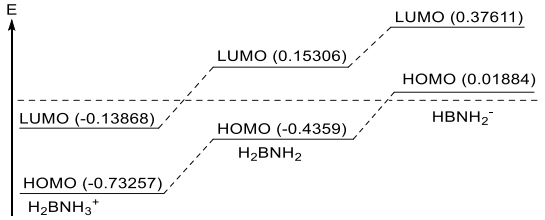

Fig. 2. HOMO and LUMO energy diagrams of $H_2BNH_3^+$, H_2BNH_2 and $HBNH_2^-$ species calculated at HF/cc-pvdz level.

Table 3 Some quantum chemical parameters (a.u.) obtained at HF/cc-pvdz level for neutral, cationic and anionic boron-nitrogen species

Compounds	B/N ratio	HOMO	LUMO	η	μ	ε	ω
1a	1/1	-0.43590	0.15306	0.58896	-0.14142	-0.08329	0.005889
2a	2/1	-0.46400	0.09341	0.55741	-0.18530	-0.10329	0.009569
3a	1/2	-0.36976	0.19188	0.56164	-0.08894	-0.04995	0.002221
4a	1/1	-0.40114	0.13551	0.53665	-0.13282	-0.07128	0.004733
4b	1/1	-0.39828	0.12432	0.52260	-0.13698	-0.07159	0.004903
5a	2/3	-0.36500	0.18545	0.55045	-0.08978	-0.04942	0.002218
5b	2/3	-0.36446	0.18490	0.54936	-0.08978	-0.04932	0.002214
5c	2/3	-0.36757	0.17255	0.54012	-0.09751	-0.05267	0.002568
6a	3/2	-0.42768	0.10297	0.53065	-0.16236	-0.08615	0.006994
6b	3/2	-0.42550	0.09885	0.52435	-0.16333	-0.08564	0.006994
6c	3/2	-0.41975	0.10073	0.52048	-0.15951	-0.08302	0.006621
$1a^+$	1/1	-0.73257	-0.13868	0.59389	-0.43563	-0.25871	0.056351
$2a^+$	2/1	-0.71763	-0.15698	0.56065	-0.43731	-0.24518	0.053608
$3a^+$	1/2	-0.64178	-0.04748	0.59430	-0.34463	-0.20481	0.035292
$4a^+$	1/1	-0.63086	-0.07497	0.55589	-0.35292	-0.19618	0.034618
$4b^+$	1/1	-0.64864	-0.08839	0.56025	-0.36852	-0.20646	0.038042
$5a^+$	2/3	-0.61817	-0.04420	0.57397	-0.33119	-0.19009	0.031478
$5b^+$	2/3	-0.61817	-0.04420	0.57397	-0.33119	-0.19009	0.031478
$5c^+$	2/3	-0.61955	-0.02987	0.58968	-0.32471	-0.19147	0.031087
$6a^+$	3/2	-0.62446	-0.11778	0.50668	-0.37112	-0.18804	0.034893
$6b^+$	3/2	-0.64124	-0.11729	0.52395	-0.37927	-0.19872	0.037683
$6c^+$	3/2	-0.66432	-0.10231	0.56201	-0.38332	-0.21543	0.041288
$1a^-$	1/1	0.01884	0.37611	0.35727	0.197475	0.070552	0.006966
$2a^-$	2/1	-0.01199	0.29194	0.30393	0.139975	0.042543	0.002977
$3a^-$	1/2	0.01581	0.38003	0.36422	0.197920	0.072086	0.007134
$4a^-$	1/1	-0.00918	0.31602	0.32520	0.153420	0.049892	0.003827
$4b^-$	1/1	-0.00943	0.30833	0.31776	0.149450	0.047489	0.003549
$5a^-$	2/3	0.00174	0.32366	0.32192	0.162700	0.052376	0.004261
$5b^-$	2/3	-0.00461	0.35552	0.36013	0.175455	0.063187	0.005543
$5c^-$	2/3	-0.00253	0.34363	0.34616	0.170550	0.059038	0.005034
$6a^-$	3/2	-0.03246	0.27927	0.31173	0.123405	0.038469	0.002374
$6b^-$	3/2	-0.03292	0.27591	0.30883	0.121495	0.037521	0.002279
$6c^-$	3/2	-0.03022	0.29167	0.32189	0.130725	0.042079	0.002750

The chemical hardness rankings are inversely proportional with HOMO and LUMO energy rankings for a certain compound (Table 3). Namely, the cationic species have higher chemical hardness than the neutral and anionic species. This is expected situation. Because, the chemical hardness is related to molar volume. The chemical hardness increases with the decreasing of the molar volume. The ω and ε values were calculated for the 33-chemical species by using their η and μ values. The correlation between the ε and ω values of the 33-chemical species was presented in Fig. 3.

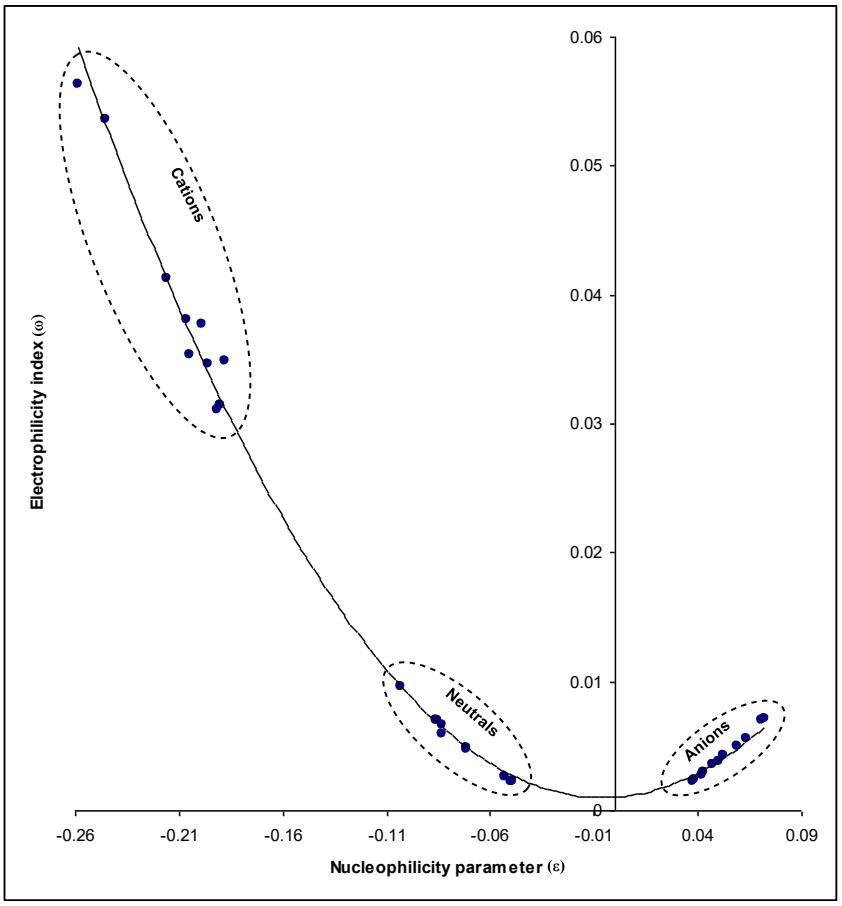

Fig. 3. The ω-ε correlation for the 33-chemical species.

Fig. 3 shows that the cationic and neutral species have negative ε values, whereas the anionic species have positive ε values. The ω values of the cationic species are higher than the neutral and anionic species. Regression analysis of the ω-ε correlation gave a second order parabolic curve. The equation of this parabolic curve is

$$\omega = 0.9077\varepsilon^2 + 0.0103\varepsilon + 0.001 \quad (R^2=0.996)$$

The correlation coefficient (R^2) of the ω-ε relation is very close to 1. This result showed that there is a good correlation between the ω and ε values in the second order parabolic curve. If the ε values of any other boron-nitrogen open-chain compounds are known, the ω values can be calculated from this parabolic curve equation. As can be seen from Fig. 3, the ω values of the cationic and neutral species are in the same tendency. Therefore, B/N ratio-ω correlation was investigated for the neutral and anionic species. This correlation was given in Fig.4.

As can be seen from Fig. 4, generally the ω values of the neutral compounds are increasing with increasing of B/N ratio. The higher B/N ratio means that the number of acceptor boron atoms are increased. The ω values are increasing with increasing the number of acceptor boron atoms for the neutral species. whereas the ω values of the anionic species are decreasing with increasing of B/N ratio. This situation can be explained by separation of the proton from the most positively charged boron atom. The boron atom would thus have negative formal charge. Having more negative formal charge species will have lower ω values.

3.4 Proton affinities of neutral and anionic species

PA values were calculated from the energy differences between the interested molecule and the same molecule with one additional proton. For example, the PA values of the BH_2NH_2 and

$BHNH_2^-$ species can be calculated from the following equations.

$$PA_{(BH_2NH_2)} = E_{(BH_2NH_2)} - E_{(BH_2NH_3^+)} \quad (9)$$

$$PA_{(BHNH_2^-)} = E_{(BHNH_2^-)} - E_{(BH_2NH_2)} \quad (10)$$

where E is the sum of the electronic and thermal energies of the related species. The PA values of the neutral and anionic boron-nitrogen open chain were given in Table 4.

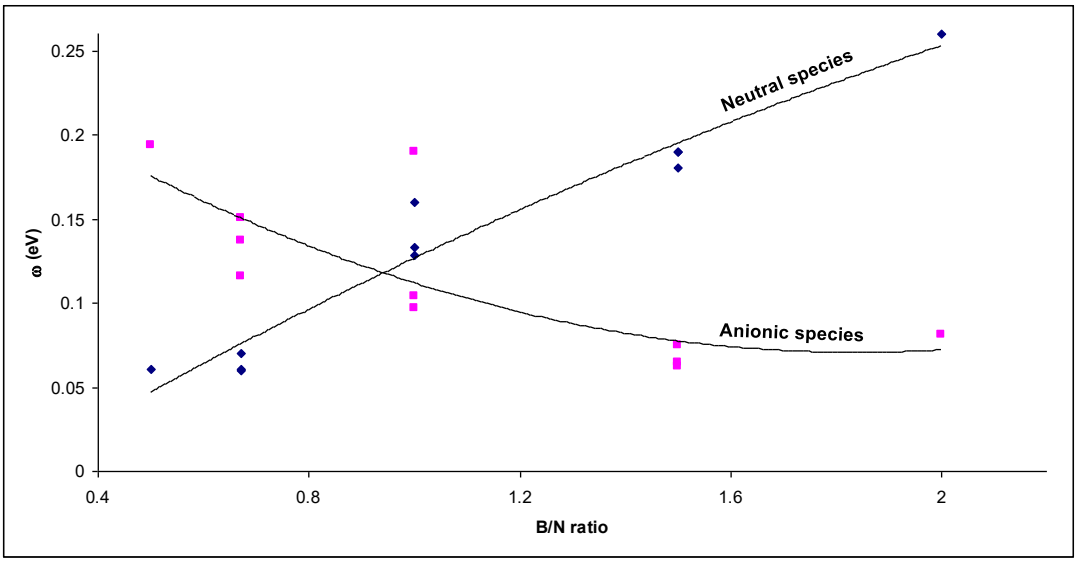

Fig. 4. B/N ratio-ω correlation for the neutral and anionic species.

As can be seen from Table 4, The PA values of the anionic species are higher than the neutral species. The PA values of the neutral species vary from 7 to 10 eV while the PA values of the anionic species are within the range 18-20 eV. These findings indicate that the anionic species have the more basic character than the neutral species. These values are also compatible with HOMO-LUMO energy rankings given in Fig 2. The rankings of PA values for the neutral or anionic species should be associated with B/N ratio or ω values. The PA-B/N ratio and PA-ω relations were investigated for the neutral and anionic species. These relations were given in Fig. 5.

The PA values for the neutral species increase with decreasing of B/N ratio and ω values (Fig 5). The lower B/N ratio means the higher nitrogen number. Nitrogen atoms are electron donor due to the lone pair on the nitrogen atoms. Therefore, PA values and alkalinity of neutral species increase with decreasing of B/N ratio. The PA-ω relation for the neutral species are the same tendency with the relation of PA-B/N ratio. Namely, PA values and alkalinity increase with decreasing of the ω values. This is expected situation. Because, proton is an electrophile and it interacts more strongly with high nucleophilic species. High nucleophilic species have lower ω values. Thus, PA values increase with decreasing of the ω values.

Generally, PA values for the anionic species increase with decreasing of B/N ratio, whereas PA values for anionic species increase with increasing of the ω values (Fig. 5). The PA-B/N ratio relation can be explained as in the neutral species. The PA-ω relationship for anionic species is opposite to those in the neutral species. This is due to increase in the number of electrons per the nucleus. Thus, PA values and alkalinity increase with increasing of the ω values.

Table 4. ω (eV) and PA (eV) values for the neutral and anionic species

Neutral				Anionic			
Species	B/N ratio	ω	PA	Species	B/N ratio	ω	PA
1a	1/1	0.160218	8.134377	$1a^-$	1/1	0.189506	19.20151
2a	2/1	0.260318	7.537820	$2a^-$	2/1	0.080999	18.64219
3a	1/2	0.060430	9.142367	$3a^-$	1/2	0.194064	19.41060
4a	1/1	0.128762	8.725493	$4a^-$	1/1	0.104116	18.90564
4b	1/1	0.133379	8.825277	$4b^-$	1/1	0.096537	18.95343
5a	2/3	0.060344	8.967935	$5a^-$	2/3	0.115911	19.24046
5b	2/3	0.060231	9.004334	$5b^-$	2/3	0.150797	19.02343
5c	2/3	0.069854	9.092611	$5c^-$	2/3	0.136957	19.14890
6a	3/2	0.190258	7.874470	$6a^-$	3/2	0.064572	18.48816
6b	3/2	0.190252	7.955919	$6b^-$	3/2	0.062007	18.50821
6c	3/2	0.180129	8.327008	$6c^-$	3/2	0.074822	18.48914

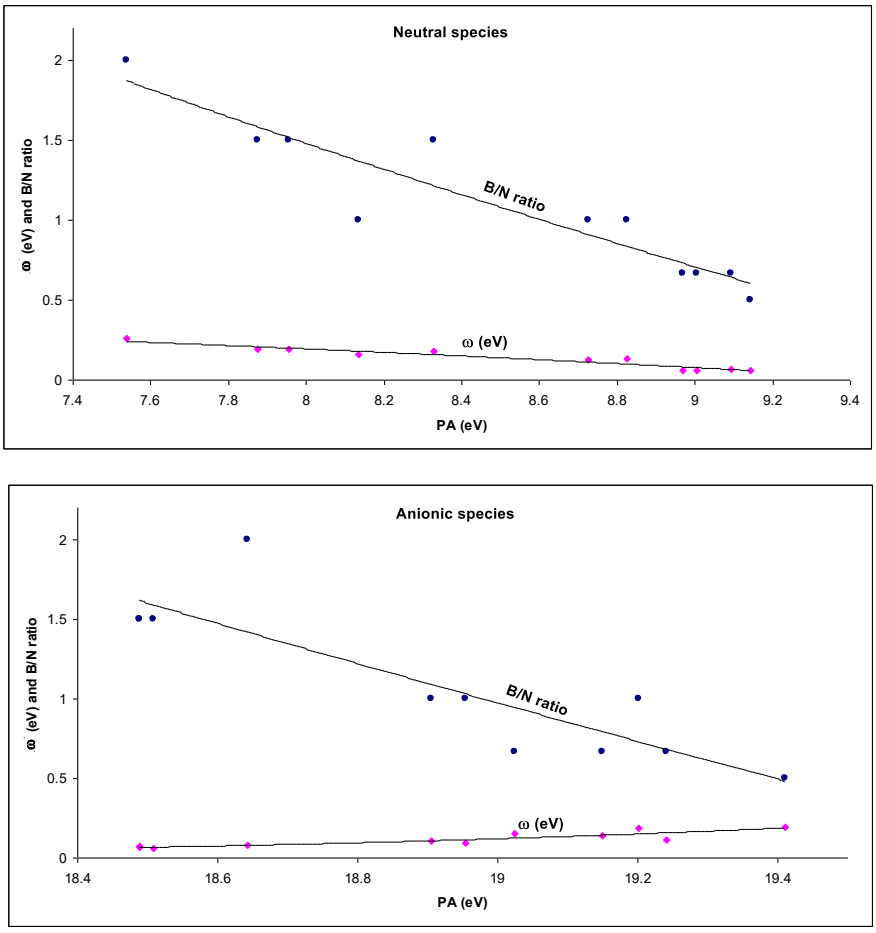

Fig. 5. The PA-B/N ratio and PA-ω relations for the neutral and anionic species.

4. Conclusion

Electrophilicity indexes (ω) and nucleophilicity parameters (ε) were calculated for the 33 boron-nitrogen open-chain species. A parabolic curve was obtained from the graph of the ε against to ω. An equation was derived to calculate the ω values of the boron-nitrogen open-chain species. The correlation ω-B/N ratio was examined. It was found that the ω values of the neutral species increased with increasing of B/N ratio, and the ω values of the anionic species decreased with increasing of B/N ratio. Proton affinities (PA) were calculated for the

comparison of the basicity of the neutral and anionic species. PA values of the anionic species are higher than the neutral species. The PA-B/N ratio and PA-ω relations were investigated. It was found that the PA values of neutral and anionic species increased with decreasing of B/N ratio. PA values of the neutral species increased with decreasing of the ω values, whereas PA values for the anionic species increased with increasing of the ω values.

Acknowledgments

We are grateful to the unit of scientific research projects of Cumhuriyet University for financial supports (Project No: F-308)

References

[1] J. Zhang, Q. Shu Li, S. Zhang, Theoretical study on the structures of boron–nitrogen alternant open chain compounds, Journal of Molecular Structure: THEOCHEM 715 (2005) 133–141.

[2] R. G. Parr, R. A. Donnelly, M. Levy, W. E. Palke, The Journal of Chemical Physics 68 (1978) 3801-3807.

[3] R. G. Parr, R. G. Pearson, Absolute hardness: companion parameter to absolute electronegativity, J. Am. Chem. Soc. 105 (1983) 7512-7516.

[4] T. A. Koopmans, Über die Zuordnung von Wellenfunktionen und Eigenwerten zu den Einzelnen Elektronen Eines Atoms, Physica 1 (1933) 104-113.

[5] R. G. Pearson, The principle of maximum hardness, Accounts of Chemical Research 26 (1993) 250-255.

[6] R. G. Pearson, Chemical hardness and density functional theory, Journal of Chemical Sciences 117 (2005) 369-377.

[7] R. G. Parr, L. V. Szentpaly, S. Liu, J. Am. Chem. Soc. 121 (1999) 1922-1924.

[8] S. Kiyooka, D. Kaneno, R. Fujiyama, Parr's index to describe both electrophilicity and nucleophilicity, Tetrahedron Letters 54 (2013) 339–342.

[9] J. E. Huheey, E. A. Keitler, R. L. Keitler, O. K. Mehdi, Inorganic Chemistry, Principles of Structure and Reactivity, Fourth Edition, Pearson, 1993, 223.

[10] R. D. Dennington II, T. A. Keith, J. M. Millam, GaussView 5.0.8, Wallingford, CT, (2009)

[11] M. J. Frisch, G. W. Trucks, H. B. Schlegel, G. E. Scuseria, M. A. Robb, J. R. Cheeseman, G. Scalmani, V. Barone, B. Mennucci, G. A. Petersson, H. Nakatsuji, M. Caricato, X. Li, H. P. Hratchian, A. F. Izmaylov, J. Bloino, G. Zheng, J. L. Sonnenberg, M. Hada, M. Ehara, K. Toyota, R. Fukuda, J. Hasegawa, M. Ishida, T. Nakajima, Y. Honda, O. Kitao, H. Nakai, T. Vreven, J. A. Montgomery Jr., J. E. Peralta, F. Ogliaro, M. Bearpark, J. J. Heyd, E. Brothers, K. N. Kudin, V. N. Staroverov, R. Kobayashi, J. Normand, K. Raghavachari, A. Rendell, J. C. Burant, S. S. Iyengar, J. Tomasi, M. Cossi, N. Rega, J. M. Millam, M. Klene, J. E. Knox, J. B. Cross, V. Bakken, C. Adamo, J. Jaramillo, R. Gomperts, R. E. Stratmann, O. Yazyev, A. J. Austin, R. Cammi, C. Pomelli, J. W. Ochterski, R. L. Martin, K. Morokuma, V. G. Zakrzewski, G. A. Voth, P. Salvador, J. J. Dannenberg, S. Dapprich, A. D. Daniels, Ö. Farkas, J. B. Foresman, J. V. Ortiz, J. Cioslowski, D. J. Fox, Gaussian 09, Revision A.02, Gaussian, Inc., Wallingford CT (2009)

[12] J. A. Pople, R. K. Nesbet, Self-Consistent Orbitals for Radicals, The Journal of Chemical Physics 22 (1954) 571.

[13] A. D. Becke, Density-functional thermochemistry. III. The role of exact exchange, The Journal of Chemical Physics 98 (1993) 5648-5652.

[14] C. Lee, W. Yang, R. G. Parr, Development of the Colle-Salvetti correlation-energy formula into a functional of the electron density, Physical Review B 37 (1988) 785-789.

[15] M. J. Frisch, M. Head-Gordon, J. A. Pople, A direct MP2 gradient method, Chemical Physics Letters 166 (1990) 275-280.

[16] M. Head-Gordon, J. A. Pople, M. J. Frisch, MP2 energy evaluation by direct methods, Chemical Physics Letters 153 (1988) 503-506.

[17] T.H. Dunning Jr, Gaussian basis sets for use in correlated molecular calculations. I. The

atoms boron through neon and hydrogen, The Journal of Chemical Physics 90 (1989) 1007-1023.

[18] R.A. Kendall, T.H. Dunning Jr, R.J. Harrison, Electron affinities of the first-row atoms revisited. Systematic basis sets and wave functions, The Journal of Chemical Physics 96 (1992) 6796-6806.

[19] D.E. Woon, T.H. Dunning Jr, Gaussian basis sets for use in correlated molecular calculations. III. The atoms aluminum through argon, The Journal of Chemical Physics 98 (1993) 1358-1371.

[20] Ş. Güveli, N. Özdemir, T. Bal-Demirci, B. Ülküseven, M. Dinçer, Ö. Andaç, Quantum-chemical, spectroscopic and X-ray diffraction studies on nickel complex of 2-hydroxyacetophenone thiosemicarbazone with triphenylphospine, Polyhedron 29 (2010) 2393–2403

[21] K. Sayın, D. Karakaş, Quantum chemical studies on the some inorganic corrosion inhibitors, Corrosion Science 77 (2013) 37-45.

Turkish Computational and Theoretical Chemistry

Turkish Comp Theo Chem (TC&TC)

Volume(Issue): 1(1) – Year: 2017 – Pages: 11-16

Received: 13.03.2017 ***Accepted:*** 25.03.2017 *Research Article*

Theoretical Investigation of Temperature Effect on the Formation of Sulphuric Acid Rain

Koray SAYIN[1], Duran KARAKAŞ

Cumhuriyet University, Science Faculty, Chemistry Department, 58140 Sivas / Turkey

Abstract: The acid rain is a major problem for life and environment. Mainly, acid rain consists from sulfuric acid and nitric acid. There are five successive reaction for the formation of sulfuric acid. All reactions have been investigated experimentally but some properties of them have not been defined clearly. In this study, mechanisms of each reaction were predicted. The temperature effect on activation energy, equilibrium constant and rate constant were investigated for each reaction. The effect of global warming on the formation of sulphuric acid rain was discussed.

Keywords: *Acid rain, Sulfuric acid, Atmospheric reactions, Theoretical study, Global warming*

1. Introduction

Acid rain has a special importance since time immemorial and has been recognized as a threat to the environment. Acid rains are influenced from atmospheric acidic pollution [1-3] meteorology [4-6], topographic structure [7-10] and geographic position [11-12]. Acid rain is consisted from some compounds and these compounds spread with human activities such as using car, fossil fuels etc. These compounds are sulphur dioxide (SO_2), nitrogen oxides (NO_x), ammonia (NH_3), carbon monoxide (CO), carbon dioxide (CO_2), black carbon (BC) and particulate organic matter (POM) [3, 13-17]. Although these compounds spread with human activities and effect the life of the world such as soil, lakes, plants, animals, buildings and cultural heritages. Composition of acid rain is generally formed from SO_2 and NO_x. The five-successive reaction for the formation of sulfuric acid was given as following:

$$S + O_2 \rightarrow SO + O \quad (1)$$

$$SO + O_2 \rightarrow SO_2 + O \quad (2)$$

$$HO\cdot + SO_2 + N_2 \rightarrow HOSO_2\cdot + N_2 \quad (3)$$

$$HOSO_2\cdot + O_2 \rightarrow HO_2\cdot + SO_3 \quad (4)$$

$$SO_3 + H_2O \rightarrow H_2SO_4 \quad (5)$$

Different studies for each reaction have been made to determine the rate constant value. For the reaction **(1)**, rate constant (k) is equal to 2.1×10^{-12} cm^3 $molecule^{-1}$ s^{-1} at 298 K [18]. This value is average of previous reported values [19-23]. It was reported that a small decrease in rate constant was occurred with increasing temperature [23]. As for the reaction **(2)**, different rate constant values were given [24, 25]. The rate constant value is reported as 7.6×10^{-17} cm^3 $molecule^{-1}$ s^{-1} at 298 K [18]. For reaction **(3)**, rate constant values were determined in low and high pressure [26]. The rate constant value is equal to 4.1×10^{-31} cm^3 $molecule^{-1}$ s^{-1} at 298 K [18]. OH radical does not react with SO_2 in the presence of NO and O_2 [27, 28]. But $HOSO_2$ radical forms as a result of reaction **(3)**. After the reaction **(3)**, $HOSO_2$ radical reacts with oxygen gas and transforms to SO_3 as a result of reaction **(4)**. The studies on reaction **(4)** have been made to determine the rate constant value [29, 30]. For this reaction rate, constant value was found as 4.1×10^{-13} cm^3

[1] Corresponding Author

e-mail: krysayin@gmail.com and ksayin@cumhuriyet.edu.tr

molecule^{-1} s^{-1} at 298 K [18]. As for the reaction **(5)**, rate constant value is less than 6x10^{-15} cm^3 molecule^{-1} s^{-1} at 298 K [18]. At different temperatures, rate constant values are not known except for reaction **(1)**. In this study, we investigated reaction mechanisms and the temperature effect on the rate constant and the equilibrium constant in the range of 273.15 – 323.15 K for each reaction.

2. Computational Method

The input files of the atoms and molecules were prepared with GaussView 5.0.8 [31]. The ground state multiplicity was taken into account for all atoms and molecules. Calculations were made using Gaussian 09 AML64L-Revision-C.01 [32] by the Hartree-Fock (HF) method with 6-311++G(d,p) basis set. 6-311++G(d,p) is the standard and high angular momentum basis set which adds p functions to hydrogen atoms and d functions on heavy atoms. In the first step, the geometries of all reactants and products were fully optimized at the HF/6-311++G(d,p) level. In the second step, the transition states for each reaction were investigated at same level. The transition state (TS) method was used to search for the transition states of all reaction paths [33, 34]. The analyses of vibrational frequencies indicated that optimized structures of reactants and products were at stationary points corresponding to local minima without imaginary frequencies. For transition states, the imaginary frequencies were found. All calculations were performed at 273.15, 283.15, 293.15, 298.15, 303.15, 313.15 and 323.15 K. For each reaction, activation energies (E_a), reaction enthalpies (ΔH) and Gibbs free energies (ΔG) were calculated by using Eq. (1), (2) and (3), respectively.

$$E_a = E_{TS} - E_{\mathrm{Re}actant} \quad (1)$$

$$\Delta H_{\mathrm{Re}action} = \sum n\Delta H_{\mathrm{Pr}oducts} - \sum n\Delta H_{\mathrm{Re}actants} \quad (2)$$

$$\Delta G_{\mathrm{Re}action} = \sum n\Delta G_{\mathrm{Pr}oducts} - \sum n\Delta G_{\mathrm{Re}actants} \quad (3)$$

Eq. (5), derived from Eq. (4), was used to calculate the equilibrium constants [35].

$$\Delta G^\circ = -RT\ln K \quad (4)$$

$$\ln\left(\frac{K_1}{K_2}\right) = \frac{\Delta H^\circ}{R}\left(\frac{1}{T_2} - \frac{1}{T_1}\right) \quad (5)$$

where K is the equilibrium constant, R is ideal gas constant and T is temperature (K). The rate constants of reactions were calculated with Eq. (7) which is derived from Eq. (6) [35]:

$$\ln k = \frac{-E_a}{RT} + \ln A \quad (6)$$

$$\ln k_1 - \ln k_2 = \left(\frac{E_{a_2}}{RT_2}\right) - \left(\frac{E_{a_1}}{RT_1}\right) \quad (7)$$

where k is the rate constant and A is frequency factor.

3. Results and Discussion

3.1. Reaction Mechanism and Thermo-Chemical Parameters

The mentioned reactions have been investigated experimentally. But there are not theoretical studies about the mechanism of reactions. In this study, theoretical calculations were performed to explain reaction mechanism. The optimized structures of reactants, products, transition states (TS) and imaginary frequencies (IF) were obtained at HF/6-311++G(d,p) level. The results were presented in Fig. 1.

For reaction **(1)**, the optimized structures of reactants and products were obtained. The structure of transition state between reactant and product was investigated and IF value transition state is -1060.9 cm^{-1}. Negative frequency is a criterion for determining the transition state. Transition states for each reaction were found in the same way. IF values are -1030.61, -113.61, -1706.97 and -2184.98 cm^{-1} for reaction **(2)**, **(3)**, **(4)** and **(5)**, respectively. The thermo-chemical parameters provide important information about the reactions. selected parameters were listed in Table 1. Activation energies (E_A), reaction enthalpies (ΔH) and reaction Gibbs free energies (ΔG) were calculated by using Eq. (1), (2) and (3).

As can be seen from reaction enthalpies, ΔH values for reaction **(1)**, **(2)** and **(5)** are negative. This result means that these reactions are exothermic under the standard conditions. For reaction **(3)** and **(4)**, the ΔH values are zero and positive, respectively. Reaction **(4)** is endothermic. Gibbs free energy values for the reaction **(1)**, **(2)**, **(3)** and **(5)** are negative while ΔG for the reaction **(4)** is positive value. ΔG values for reaction **(3)**, **(4)** and

(5) are almost near to zero. According the ΔG values, the direction of reaction **(1)**, **(2)**, **(3)** and **(5)** is spontaneous to product while the direction of reaction **(4)** is spontaneous to reactant under the standard conditions.

Table 1. Some calculated thermo-chemical parameters at 298.15 K for reactions

Reactions	E_a (kJ mol^{-1})	ΔH (kJ mol^{-1})	ΔG (kJ mol^{-1})
(1)	15.34	-186.14	-186.20
(2)	25.43	-141.32	-156.19
(3)	6.06	0.00	-0.08
(4)	115.711	38.57	23.10
(5)	141.63	-106.72	-3.17

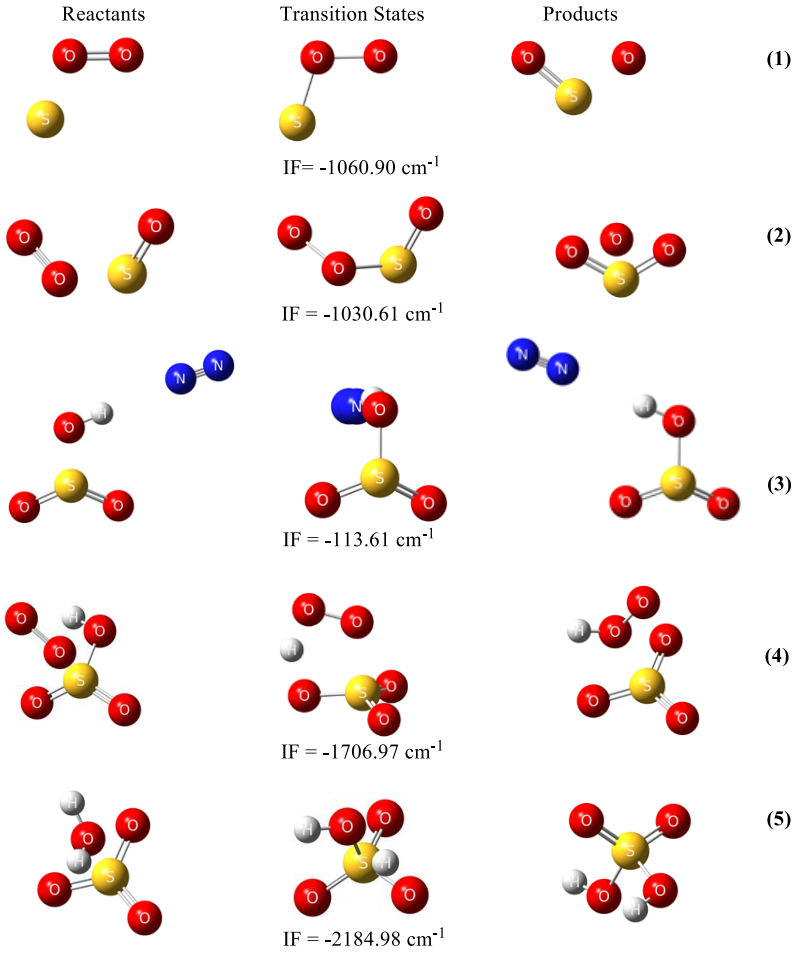

Fig. 1. Reaction mechanism of sulphuric acid formation.

3.2. The Equilibrium Constants

For all reactions, the temperature effect on the equilibrium constant was not investigated before that. Firstly, the theoretical equilibrium constant was calculated at 298.15 K and 1 atm. After that, the theoretical equilibrium constants at different temperatures were calculated by using the Eq. (5). The equilibrium constant of reactions was presented in Table 2.

According to the Table 2, the equilibrium constants generally decrease with the increasing in temperature. The equilibrium constant values of reaction **(1)** and **(2)** are higher than others. These results show that the directions of reactions are more tendency to products than reaction **(3)**, **(4)** and **(5)**. These reactions are thermodynamically stable. Their equilibrium constant decreases with increasing temperature. According to equilibrium constant of reaction **(1)** and **(2)**, it can be said that

all the reactants transform to products. For reaction **(3)**, the equilibrium constant is same value as 1.03 at different temperature. The equilibrium constant of reaction **(4)** increases with increasing temperature. The direction of reaction **(4)** is spontaneous to reactants. For reaction **(5)**, the equilibrium constant decreases with increasing temperature. Tendency to form products decreases with the increasing of temperature. Reaction **(3)** and **(5)** are almost thermodynamically stable while reaction **(4)** is unstable. Reaction **(4)** determines the formation of sulphuric acid because of its lower equilibrium constant. The formation of sulphuric acid increases slightly with increasing temperature. There is a direct correlation between global warming and the formation of sulphuric acid rain.

Table 2. The equilibrium constants at different temperatures for each reaction

Temperature (K)	Reactions				
	(1)	**(2)**	**(3)**	**(4)**	**(5)**
273.15	4.04×10^{35}	4.27×10^{29}	1.03	2.16×10^{-5}	184.9
283.15	2.23×10^{34}	4.74×10^{28}	1.03	3.93×10^{-5}	35.17
293.15	1.50×10^{33}	6.12×10^{27}	1.03	6.87×10^{-5}	7.49
303.15	1.21×10^{32}	9.04×10^{26}	1.03	1.16×10^{-4}	1.77
313.15	1.14×10^{31}	1.51×10^{26}	1.03	1.89×10^{-4}	0.46
323.15	1.25×10^{30}	2.81×10^{25}	1.03	2.99×10^{-4}	0.13

3.3. The temperature effect on activation energies and the rate constants

Activation energy is an important parameter for the reactions. For mentioned reactions, activation energies were presented in Table 1 at 298.15 K. The activation energies at different temperature were calculated for each reaction. The temperature effect on activation energies was represented graphically in Fig. 2.

According to Figure 2, activation energies of reaction **(1)**, **(3)** and **(4)** generally decrease with increasing temperature. For reaction **(2)**, there is a fluctuation with the increasing of temperature. Activation energy is higher at 293.15 and 323.15 K while activation energies are mainly equal for other temperatures. The lastly, the activation energy of reaction **(5)** increases properly with the increasing of temperature.

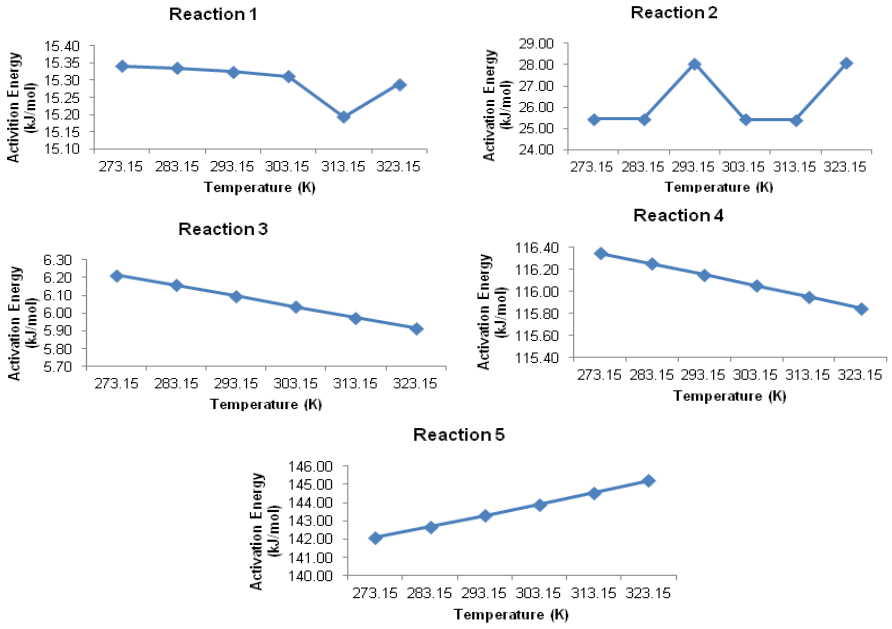

Figure 2. Graph of temperature versus activation energy for sulphuric acid formation reactions.

The rate constants at different temperatures were not investigated theoretically before that. At 298.15 K, the experimental rate constants are $2.1x10^{-17}$, $7.6x10^{-17}$, $4x10^{-31}$, $4.3x10^{-13}$ and $6x10^{-15}$ for reaction **(1)**, **(2)**, **(3)**, **(4)** and **(5)**, respectively. The rate constants at different temperature were calculated by using Eq. (7). In this equation, k_1 is experimental rate constant. Results were listed in Table 3 and rate constants of mentioned reactions generally increase with increasing temperature. These rate constants are small value. Therefore, the mentioned reactions are stable kinetically. Rate determining step is reaction **(3)** according to rate constants. Taken into account the rate constant of reaction **(3)**, it can be said that the formation of sulphuric acid rain increases with global warming.

Table 3. Rate constants (cm^3 $molecule^{-1}$ s^{-1}) at different temperature for each reaction.

Temperature (K)	Reactions				
	(1)	**(2)**	**(3)**	**(4)**	**(5)**
273.15	$1.86x10^{-17}$	$7.2x10^{-17}$	$3.93x10^{-31}$	$3.35x10^{-13}$	$4.40x10^{-15}$
283.15	$1.89x10^{-17}$	$7.4x10^{-17}$	$3.96x10^{-31}$	$3.72x10^{-13}$	$4.90x10^{-15}$
293.15	$1.91x10^{-17}$	$7.5x10^{-17}$	$3.99x10^{-31}$	$4.10x10^{-13}$	$5.50x10^{-15}$
303.15	$1.94x10^{-17}$	$7.7x10^{-17}$	$4.01x10^{-31}$	$4.58x10^{-13}$	$6.00x10^{-15}$
313.15	$1.96x10^{-17}$	$7.8x10^{-17}$	$4.03x10^{-31}$	$4.90x10^{-13}$	$6.60x10^{-15}$
323.15	$1.98x10^{-17}$	$7.5x10^{-17}$	$4.06x10^{-31}$	$5.32x10^{-13}$	$7.20x10^{-15}$

4. Conclusion

The formation of sulphuric acid, reaction mechanisms, temperature effect on some thermo-chemical parameters which are activation energies, rate constants and equilibrium constants were investigated theoretically. Transition states for each reaction and imaginary frequencies were found. The reaction enhalpies, Gibbs free energies and the activation energies of each reaction were calculated. Equilibrium constant of reaction **(4)** was obtained smaller than other steps. Its value increases with temperature. The results showed that reaction **(4)** was found as thermodynamically unstable. Rate constant of mentioned reactions were calculated and were found to increase with temperature. Rate determining step was found as reaction **(3)**. According to equilibrium and rate constants, formation of sulphuric acid was found to increase with temperature. The results indicated that sulphuric acid rain increases with global warming.

Acknowledgments

We thank office of scientific research projects of Cumhuriyet University (Project No: F-308 and F-372) for financial supports. This research was made possible by TUBITAK ULAKBIM, High Performance and Grid Computing Center (TR-Grid e-Infrastructure).

References

[1] A. A. N. Patrinos, M. J. Leach, R. M. Brown, Journal of Applied Meteorology 28 (1989) 948-968.

[2] C. Anatolaki, R. Tsitouridou, Atmospheric Research 92 (2009) 100-113.

[3] X. Zhang, H. Jiang, J. Jin, X. Xu, Q. Zhang, Atmospheric Environment 46 (2012) 590-596.

[4] J. C. Nam, S. N. Oh, J. C. Choi, J. Kim, Y. Chun, Water, Air and Soil Pollution 130 (2001) 433-438.

[5] C. C. Lin, X. M. Lin, Y. Zou,L. Zhang, Journal of Tropical Meteorology 21 (2005) 330-336.

[6] A. K. Singh, G. C. Mondal, S. Kumar, K. K. Singh, K. P. Kamal, A. Sinha, Environmental Monitoring and Assessment 125 (2007) 99-110.

[7] T. A. Hill, A. Jones, T. W. Choularton, Quarterly Journal of the Royal Meteorological Society 113 (1987) 1217-1236.

[8] T. W. Choularton, M. J. Gay, A. Jones, D. Fowler, J. N. Cape, I. D. Leith, Atmospheric Environment 22 (1988) 1363-1371.

[9] G. Sumner, Precipitation Process and Analysis. John Wiley, 1988 New York.

[10] J. W. Grimm, J. A. Lynch, Environmental Monitoring and Assessment 90 (2004) 243-268.

[11] S. V. Ollinger, J. D. Aber, G. M. Lovett, S. E. Millham, R. G. Lathrop, J. M. Ellis, Ecological Applications 3 (1993) 459-472.

[12] M. Ito, M. J. Mitchell, C. T. Driscoll, Atmospheric Environment 36 (2002) 1051-1062.

[13] J. P. Hutton, G. E. Halkos, Energy Economics 17 (1995) 259-275.

[14] L. Hordijk, C. Kroeze, Eur. J. Oper. Res. 102 (1997) 405-417.

[15] J. W. Park, S. Y. Cho, Atmospheric Environment 32 (1998) 2745-2756.

[16] B. He, X. Zheng, Y. Wen, H. Tong, M. Chen, C. Chen, J. Energy. Convers. Manage. 44 (2003) 2175-2188.

[17] V. Eyring, I. S. A. Isaksen, T. Berntsen, W. J. Collins, J. J. Corbett, O. Endresen, R. G. Grainger, J. Moldanova, H. Schlager,D. S. Stevenson, Atmospheric Environment 44 (2010) 4735-4771.

[18] R. Atkinson, D. L. Baulch, R. A. Cox, R. F. Hampson, J. A. Kerr, M. J. Rossi, J. Troe, J. Phys. Chem. Ref. Data 26 (1997) 521-1011.

[19] R. W. Fair, B. A. Thrush, Trans. Faraday Soc. 65 (1969) 1557-1570.

[20] R. W. Fair, A. V. Roodselaar, O. P. Strausz, Can. J. Chem. 49 (1971) 1659-1664.

[21] D. D. Davis, R. B. Klemm, M. J. Pilling, Int. J. Chem. Kinet. 4 (1972) 367-382.

[22] R. J. Donovan, D. J. Little, Chem. Phys. Lett. 13 (1972) 488-490.

[23] M. A. A. Clyne, P. D. Whitefield, J. Chem. Soc. Faraday Trans. 275 (1979) 1327-1340.

[24] G. Black, R. T. Shrapless, T. G. Slanger, Chem. Phys. Lett. 90 (1982) 55-58.

[25] G. Black, R. T. Shrapless, T. G. Slanger, Chem. Phys. Lett. 90 (1982) 598-602.

[26] Y. Y. Lee, W. C. Kao, Y. P. Lee, J. Phys. Chem. 94 (1990) 4535-4540.

[27] J. J. Margitan, J. Phys. Chem. 88 (1984) 3314-3318.

[28] D. Martin, J. L. Jourdain, G. Le Bras, J. Phys. Chem. 90 (1986) 4143-4147.

[29] J. F. Gleason, A. Sinha, C. J. Howard, J. Phys. Chem. 91 (1987) 719-724.

[30] J. F. Gleason, C. J. Howard, J. Phys. Chem. 92 (1988) 3414-3417.

[31] Dennington II R.D., Keith T.A., Millam J.M., 2009. Gaussview 5.0, Wallingford, CT, USA.

[32] Gaussian 09, Revision D.01, M. J. Frisch, G. W. Trucks, H. B. Schlegel, G. E. Scuseria, M. A. Robb, J. R. Cheeseman, G. Scalmani, V. Barone, B. Mennucci, G. A. Petersson, H. Nakatsuji, M. Caricato, X. Li, H. P. Hratchian, A. F. Izmaylov, J. Bloino, G. Zheng, J. L. Sonnenberg, M. Hada, M. Ehara, K. Toyota, R. Fukuda, J. Hasegawa, M. Ishida, T. Nakajima, Y. Honda, O. Kitao, H. Nakai, T. Vreven, J. A. Montgomery, Jr., J. E. Peralta, F. Ogliaro, M. Bearpark, J. J. Heyd, E. Brothers, K. N. Kudin, V. N. Staroverov, R. Kobayashi, J. Normand, K. Raghavachari, A. Rendell, J. C. Burant, S. S. Iyengar, J. Tomasi, M. Cossi, N. Rega, J. M. Millam, M. Klene, J. E. Knox, J. B. Cross, V. Bakken, C. Adamo, J. Jaramillo, R. Gomperts, R. E. Stratmann, O. Yazyev, A. J. Austin, R. Cammi, C. Pomelli, J. W. Ochterski, R. L. Martin, K. Morokuma, V. G. Zakrzewski, G. A. Voth, P. Salvador, J. J. Dannenberg, S. Dapprich, A. D. Daniels, Ö. Farkas, J. B. Foresman, J. V. Ortiz, J. Cioslowski, and D. J. Fox, Gaussian, Inc., Wallingford CT, 2009.

[33] J. Baker, J. Comp. Chem. 7 (1986) 385-389.

[34] C. Doubleday, J. Mclver, M. Page, T. Zielinski, 1985. J. American Chem. Society 107 (1985) 5800-5801.

[35] R. H. Petrucci, W. S. Harwood, F. G. Herring, edt: T. Uyar, S. Aksoy, Genel Kimya 2. Palme Yayıncılık, 2005 ANKARA.

Turkish Computational and Theoretical Chemistry

Turkish Comp Theo Chem (TC&TC)

Volume(Issue): 1(1) – Year: 2017 – Pages: 17-26

Received: 21.03.2017 ***Accepted:*** 29.03.2017 *Research Article*

CO_2 transformation on the active site of carbonic anhydrase enzyme leading to formation of H_2CO_3 - A biomimetic model through computational study

Ramasamy SHANMUGAM[a], Arunachalam THAMARAİCHELVAN[b], Balasubramanian VİSWANATHAN[a,1]

[a]National Center for Catalysis Research, Indian Institute of Technology Madras, Chennai, Tamilnadu 600 036, INDIA

[b]Faculty of Allied Health Sciences, Chettinad Academy of Research and Education, Kelambakkam, Tamilnadu 603 103, INDIA

Abstract: Maximizing the utilization of CO_2 through mimicking its activation by nature to form H_2CO_3 is considered and tested. The active site present in the carbonic anhydrase was chosen as the model and various electron releasing and withdrawing substituents were introduced in the imidazole rings to alter the activity of the enzyme model. To compare their activities, the mechanistic pathway was probed for the pure and substituted models employing DFT/B3LYP level of theory. Optimization was performed on structures and the computed energies were used for elucidating the mechanistic pathway. The study reveals that the designed active site model that mimics the nature's process, yields results similar to those observed in nature. The study will help the process of capturing and activation of CO_2 effectively to form H_2CO_3.

Keywords: *CO_2, carbonic anhydrase, DFT, H_2CO_3*

1. Introduction

In the recent years, among the various attractive fields of research, utilization of CO_2 draws more attention due to immense possibility of various products formation [1, 2]. Further, from the point of view of environmental concern, it is the right time to mitigate this global warming greenhouse gas [3]. In order to achieve this, numerous efforts have been undertaken though there is no such process with considerable efficiency.

When nature is looked upon for a solution, it is quite interesting that the enzyme carbonic anhydrase reversibly fixes the CO_2 into bicarbonate [4, 5]. This activity is mainly attributed to the specific active site of the enzyme which is made up of Zn(II) ion surrounded by three histidine units and one water molecule. In reality, the handling of these enzymes at ordinary conditions is difficult. Furthermore, it is not possible to directly use the enzyme as a catalyst for a prolonged time in a reaction.

To overcome hurdles, in handling enzymes, researchers are trying to make the active site containing inorganic complex molecules which is capable of mimicking the catalytic role of an enzyme. These kinds of studies are providing an opportunity to mimic the natural process at the laboratory level [6-8]. Recently, metal organic frame works and transition metal surfaces, exhibited prominent activity towards carbonic acid

[1] Corresponding Author

e-mail: bvnathan@iitm.ac.in

formation reaction [9, 10]. This study prompted the evaluation of such activity by the metal in the enzyme model. In general metals can convert CO_2 to CH_4, CO, HCOOH, CH_3OH, etc. It is desirable to elucidate a new path which can help to transform CO_2 into other value added products to a considerable extent. There are certain metal complexes which effectively catalyze the CO_2 transformation reactions [11-13]. These conclusions revealed that CO_2 could be transformed into various products on carbonic anhydrase. Furthermore, zeolitic imidazole framework (ZIFs) systems, having coordinatively unsaturated metal sites at the end of the corners or surfaces, behave as photocatalysts [14-16] in CO_2 transformation. The above study suggests the view that ZIFs can effectively support the transformation of CO_2.

To achieve effective conversion of CO_2 into H_2CO_3, the active site of the enzyme model was considered. Further, effect of various electron releasing and withdrawing groups was also studied. All these evaluations were carried out using quantum mechanical methods at DFT/B3LYP level.

2. Computational Methods

Geometry optimization and other energy related calculations were performed using Hybrid density functional of B3LYP level of theory. Core electrons in the Zn atom were treated at LANL2DZ level of basis set. Basis set of 6-31g(d) was used for the electrons in all other elements such as C, O, N and H. After initial geometry optimization, stability was further evaluated by calculating the single point energy along with vibrational frequency calculations to find out whether the obtained configurations were in stationary or transition/intermediate states. The interaction between the model and the reactant were evaluated by calculating the binding energy between them. Binding energy (BE), is given by $BE = E_{model+reactant} - E_{model} - E_{reactant}$, where, $E_{model+reactant}$, E_{model} and $E_{reactant}$ are the zero point energy corrected total electronic energy of the model with reactant, pure model and the reactant respectively. The reaction pathway was estimated through determination of the relative Gibbs free energy, $\Delta G = \Sigma G_{products} - \Sigma G_{reactants}$, where, $G_{products}$ and $\Sigma G_{reactants}$ are the zero-point energy corrected Gibbs free energy of the products and reactants respectively at 1 atm pressure and a temperature of 298.15 K. All the electronic structure calculations were carried out using Gaussian 09 software package [17].

3. Results and Discussion

Active site model

Careful analysis of the carbonic anhydrase enzyme reveals that its active site consists of a Zn^{2+} ion which is surrounded by three histidine (substituted imidazole) units and a water molecule to satisfy the valencies of the tetrahedral geometry (Fig.1.a). The active site of the model under study was slightly modified from the original structure in that the histidine unit consists of imidazole and a substituent. In the considered model, the substituent of the imidazole unit was replaced by methyl group. Two-dimensional representation of the modified model is shown in Fig.1. and the schematic representation of the activity of the enzyme is represented in Fig.2.

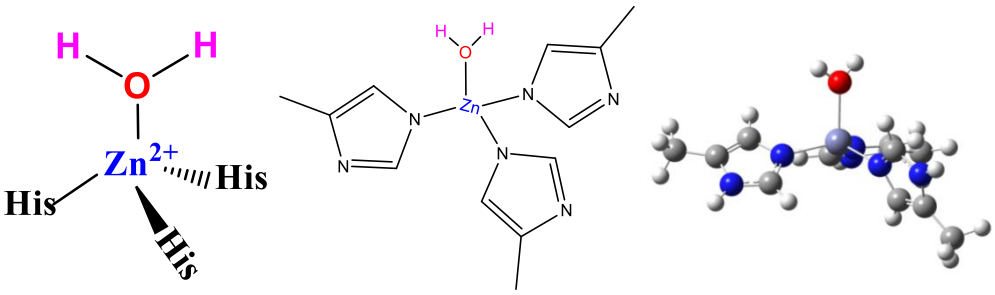

(a) **(b)** **(c)**

Fig. 1. Active site of carbonic anhydrase (a) actual site in enzyme (b) 2-D representation of the model and (c) ball and bond type representation.

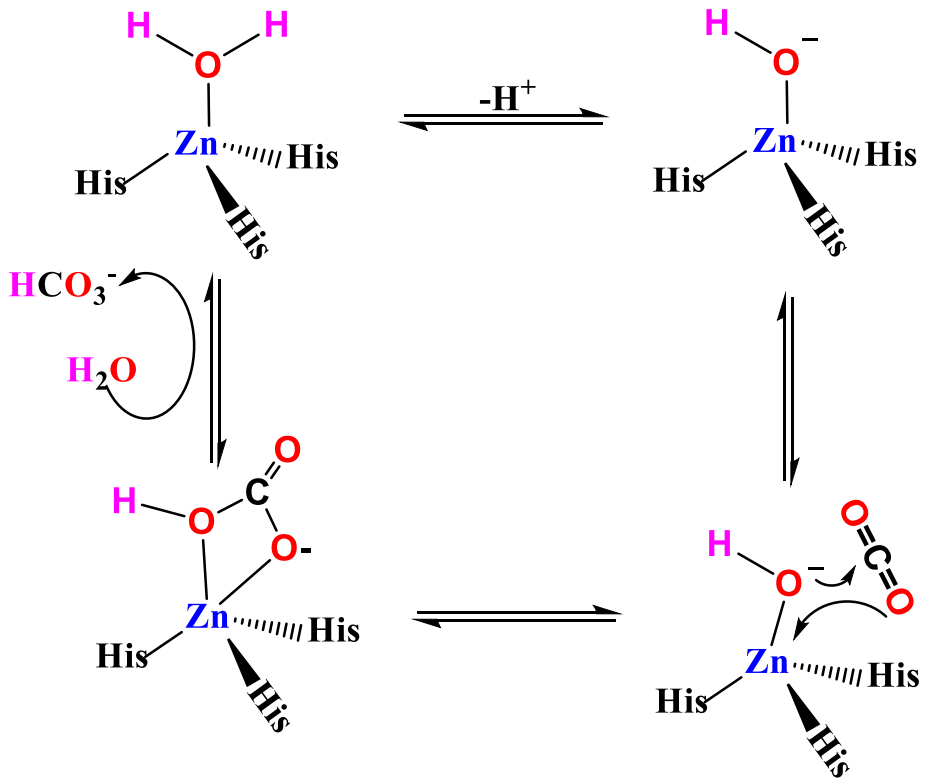

Fig. 2. Schematic representation of the activity of the enzyme in the transformation of CO_2 to H_2CO_3

The structural parameters of the constructed model are presented in Table 1. The values in the tables closely resemble with those found in earlier report [18]. Hence, the present study mainly concentrates on elucidating the nature of CO_2 interaction rather than the structural aspects.

Adsorption of CO_2 on model active site

Prior to the study on the mechanistic pathway of CO_2 transformation, initial assessment of the interaction between CO_2 & H_2O and the active site were evaluated, since, in carbonic anhydrase, all the events take place at the site containing H_2O. This is done with a view to provide clear insight into how the CO_2 gets adsorbed and activated. The possible interaction modes of CO_2 on the active site are as shown in Fig.3.

Table 1. Selected structural parameters of the active site model

Bond length	(Å)	Bond angle	(°)
Zn-O	2.13	O-H-O	106.89
Zn-N1	2.06	O-Zn-N1	100.94
Zn-N2	2.05	O-Zn-N2	103.40
Zn-N3	2.05	O-Zn-N3	107.82
O-H[a]	0.97		
O-H[b]	0.97		

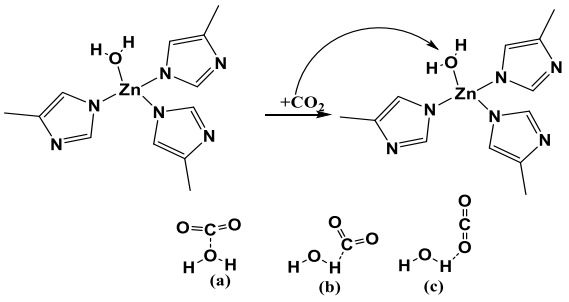

Fig. 3. Possible interaction modes of CO_2 with H_2O in the active site of the chosen model

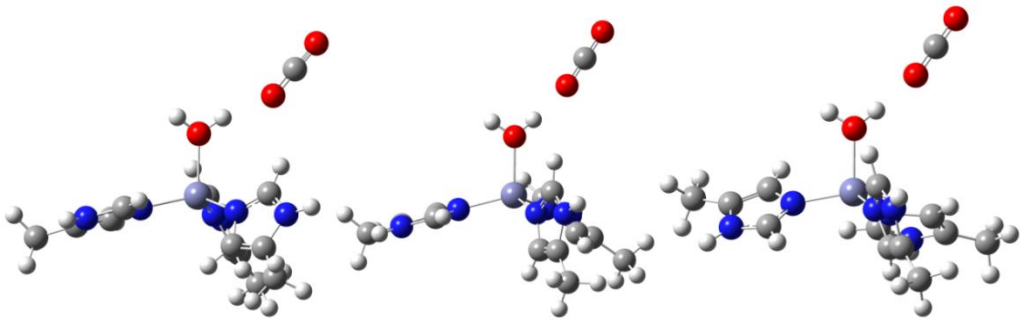

(a) **(b)** **(c)**

Fig. 4. The optimized configurations of the CO_2 interaction modes

During the interaction, three different ways of adsorption are possible for CO_2 with H_2O that are presented in Fig.3(a-c). They are: (a) C of CO_2 interacting with O of H_2O, (b) C of CO_2 orient towards H of H_2O and (c) O of CO_2 approaches towards H of H_2O. These possible interaction modes were initially subjected to geometry optimization, the resultant configurations of which are presented in Fig.4(a-c). From the figure it is clear that, the configurations of CO_2 in all the modes finally retain the linear shape rather than to expected new shape which is evident from the angle of 179.5° for CO_2. The structural parameters and the binding energy of these configurations are listed in Table 2. Further, the CO_2 interacts in all the modes in a similar way through O of CO_2 with H of H_2O at a distance of ~1.85 Å. Although, the angle of O---H-O is 177.44° which is closer to 180° supports the existence of hydrogen bonding.

Deprotonation of H_2O

The carbonic anhydrase reaction pathway is initiated by the removal of H^+ form H_2O via deprotonation step. Although, pure carbonic anhydrase itself is ready to loose H^+, the result of model-CO_2 interaction reveals that one of the oxygens of CO_2 interacts with the H of H_2O to increase the reactivity of the H^+ in comparison to the pure model. Hence, the proton removed during the deprotonation, may also directly migrate to the O of CO_2 to form COOH species. In order to verify this possibility, the COOH species was located at the point where the CO_2 was held physically. On optimization, the proton of COOH was found to migrate to OH forming H_2O and physisorbed CO_2 leading to a structure similar to that obtained in the interaction studies (Fig.4(a)). This result proves that, even though CO_2 may approach H_2O, it won't take up H^+. Hence, it is essential to elucidate the most favorable route for the deprotonation step. Thus, the deprotonation was carried out (i) in the absence of CO_2 and (ii) in presence of CO_2. For both the reactions, the calculated Gibbs free energies were arrived at as -8.02 eV and -7.72 eV respectively. The data reveal that the deprotonation is more favorable in the absence of CO_2, than in the presence of CO_2. Furthermore, the negative sign with higher values suggests that the deprotonation is a spontaneous step. As CO_2 reduces the space available for depronation the free energy decreases in the presence of CO_2. Hence, it may be concluded that the deprotonation step is an independent step.

Table 2. Binding energy (eV) and structural parameters of the CO_2 and H_2O

Optimized configurations	Binding Energy	^{a}H-O (Å)	^{b}H-O (Å)	H-O-H (°)	^{a}O-C (Å)	^{b}O-C (Å)	O-C-O (°)	^{a}O---H^a (Å)
a	-0.29	0.97	0.97	107.42	1.18	1.16	179.48	1.87
b	-0.29	0.98	0.97	106.98	1.18	1.16	179.58	1.85
c	-0.31	0.98	0.97	107.02	1.17	1.15	179.59	1.84

Interaction of CO_2 with OH

In general, the CO_2 directly interacts with OH^- to form HCO_3^- species in the five-coordinated zinc environment of the carbonic anhydrase. To verify this, the CO_2 was placed on OH^- via physisorption and chemisorption modes and then was allowed for relaxation. The result obtained indicates that, configuration of CO_2 in both the modes gets changed and both the final configurations are the same which are presented in Fig.5. The distance between the CO_2 and OH indicates that CO_2 is held by physical adsorption which is further supported by the binding energy value of -0.02 eV.

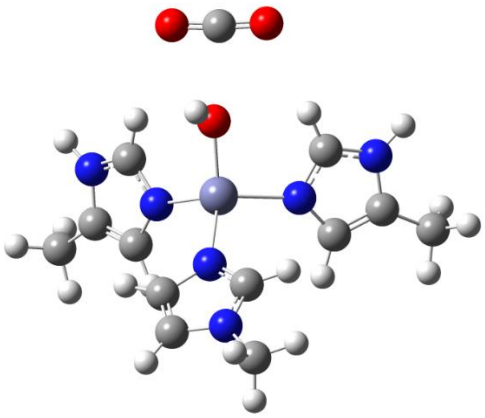

Fig. 5. Optimized structure of CO_2 with deprotanated active site

The active site in the actual enzyme is surrounded by other amino acids and peptide linkages that may facilitate the unusual coordination environment for the reported mechanism. Here, the chosen model does not include the extra environmental interactions. Further, this reactivity is totally different from the proposed usual enzyme activity. However, this study would provide guidelines for the designing of new catalysts to mimic nature's role in CO_2 transformation.

Adsorption of COOH

The dissociated proton, which is present in the medium would be easily added to the CO_2 to form $(COOH)^+$ species which then interacts with the OH^- site in the enzyme model to form H_2CO_3 species. It is interesting to note that in the case of real enzyme, H_2CO_3 is formed by the desorption of HCO_3^- from the active site which further reacts with the H^+ available in the environment. The H_2CO_3 formed from the model active site was allowed for energy minimization and the resultant configuration is presented in Fig.6. The distance of Zn-O was found to be 2.32 Å, which is 0.19 Å higher than that in the pure model. Furthermore, the H_2CO_3 unit does not move far away; but still it is interacting with the active site. This interaction was further probed with the help of binding energies. The value of -0.39 eV is obtained as binding energy for the above interaction. This energy reveals that the molecule is held on to the active site through physical adsorption. Now, it is essential to analyze whether water will be able to replace H_2CO_3 or not. In order to achieve this, the binding energy of H_2O was calculated and the value was -1.31 eV. The binding energy indicates that, H_2O can easily replace the physisorbed H_2CO_3 from the active site.

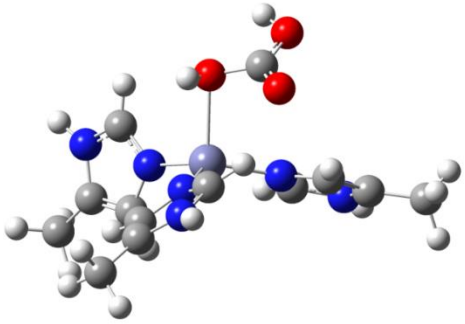

Fig. 6. Optimized structure of H_2CO_3 with the active site

Effect of Substituents in the activity of the Enzyme model

a) Gibbs free energy of formation

As seen from the earlier results, the model mimics the active site activity.

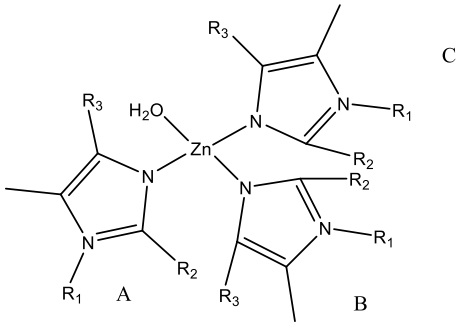

Fig. 7. 2-D Representation of the active site with the various possible substitution sites.

The imidazole moiety was substituted with different R_1, R_2 and R_3 to predict the possible change of the activity of the active site. In general, the activity of any molecule can be easily altered by substituting H of the imidazole by electron releasing and withdrawing groups. The substituents introduced and their complex formation energies are presented in Table 3. While R=Me and Et, they are electron releasing groups and hence release electrons towards the ring.

In turn, the electron density of ligating 'N' of imidazole increases, thus stability of the complexes increases. Where R=NO_2, the electron withdrawing nature of NO_2 depletes electron to make the nitrogen less basic. Hence the complexes formation energy slightly decreases as compared to that of electron releasing groups. NO_2 in position of R_2 makes the steric hindrance without H-bonding, whereas, when it is in R_3, it leads to steric hindrance though H-bonding with H of H_2O may increase the stability of the complex. Hence, NO_2 at R_3 position is more stable than R_2. In the case of halogens, electronegativity plays important role, though the size makes the electron repulsion caucuses the mesomeric effect. This leads to the increase in formation energies in the order, F>Cl>Br. On N-X, resonance effect decreases due to larger & smaller orbital overlap. So, electron density on nitrogen increases. Hence, ligation tendency increases. While comparing the formation energies in N-NO_2 and N-NO, the N-NO has less energy than N-NO_2. This is due to the fact that N-NO has resonance stabilization than N-NO_2, and hence the electrons are not readily available for the effective bonding. Fig. 7**.** Shows the 2D representation of the active site along with the positions of substituents. The electron releasing groups chosen were CH_3- and CH_3CH_2- and electron withdrawing substituents F, Cl, Br, NO_2 and NO groups were considered. Once the substituents were introduced, their thermodynamic Gibbs free energy of formation were calculated which are presented in Table 3.

The Gibbs free energies of formation of the substituted models reveal that all the model sites are thermodynamically favorable and are spontaneous in nature except for the model-19. Since, it has three bigger sized bromine atoms which are present together, the available space in the active site is less due to steric hindrance causing the formation energy as endothermic.

b) Gibbs free energy of deprotonation

The substituent effect on the enzyme model is evaluated by means of predicting the Gibbs free energy of deprotonation step and the second step of the interaction between the CO_2 and OH^- species as these two steps, at the initial stage control the whole of the mechanistic pathway. Hence, Gibbs free energies of the deprotonation have been calculated and are presented in Table 4. All the values have negative sign indicating that the process is thermodynamically feasible. While comparing the deprotonation of substituted models with that of the pure model, most of the models return slightly higher Gibbs free energy than that the pure model.

c) Interaction of CO_2 with OH^-

The interaction of CO_2 with the formed OH^- species was then evaluated. Here, the CO_2 is interacting with the modified models which are similar to the interaction in the pure model. On energy minimization, the calculated binding energy between the model and CO_2 is presented in Table 4. It is quite interesting to see that the values indicate that all the models can up take CO_2 with negative binding energies. Furthermore, the values are almost in the same range except for models 1, 9, 13, 18 & 19. Thus, the CO_2 is held physically as observed in the pure model. However, the models, 1, 9, 13, 18 &19 appear to have higher binding energies compare to other models and hence CO_2 is strongly chemisorbed in them. The chemisorption modes of adsorption of CO_2 on models 1, 9 & 13 are shown in Fig. 8.

Table 3. Various substituents of the model and their Gibbs free energy of formation

S.No (model)	Substituents									ΔG (eV)
	A			B			C			
	R^1	R^2	R^3	R^1	R^2	R^3	R^1	R^2	R^3	
1	CH_3	H	H	H	H	H	H	H	H	-21.50
2	H	H	H	CH_3	H	H	CH_3	H	H	-21.64
3	H	H	H	H	H	H	H	H	H	-21.78
4	ethyl	H	H	H	H	H	H	H	H	-21.60
5	H	H	H	ethyl	H	H	H	H	H	-21.74
6	H	H	H	H	H	H	ethyl	H	H	-21.96
7	ethyl	H	H	H	H	H	ethyl	H	H	-21.78
8	ethyl	H	H	H	H	H	CH_3	H	H	-21.72
9	ethyl	H	H	CH_3	H	H	H	H	H	-21.71
10	ethyl	H	H	ethyl	H	H	H	H	H	-21.76
11	H	F	H	H	H	H	H	H	H	-21.08
12	H	H	H	H	F	H	H	H	H	-21.02
13	H	H	H	H	H	H	H	F	H	-21.05
14	H	F	H	H	F	H	H	F	H	-20.33
15	H	F	H	H	F	H	H	H	H	-20.71
16	H	F	H	H	H	H	H	F	H	-20.71
17	H	H	H	H	F	H	H	F	H	-20.73
18	H	Cl	H	H	Cl	H	H	Cl	H	-18.97
19	H	Br	H	H	Br	H	H	Br	H	6.523
20	H	H	F	H	H	F	H	H	F	-21.47
21	H	H	Cl	H	H	Cl	H	H	Cl	-21.07
22	H	H	NO_2	H	H	NO_2	H	H	NO_2	-19.51
23	H	NO_2	H	H	NO_2	H	H	NO_2	H	-17.11
24	F	H	H	F	H	H	F	H	H	-76.55
25	Cl	H	H	Cl	H	H	Cl	H	H	-75.37
26	Br	H	H	Br	H	H	Br	H	H	-74.76
27	NO	H	H	NO	H	H	NO	H	H	-12.53

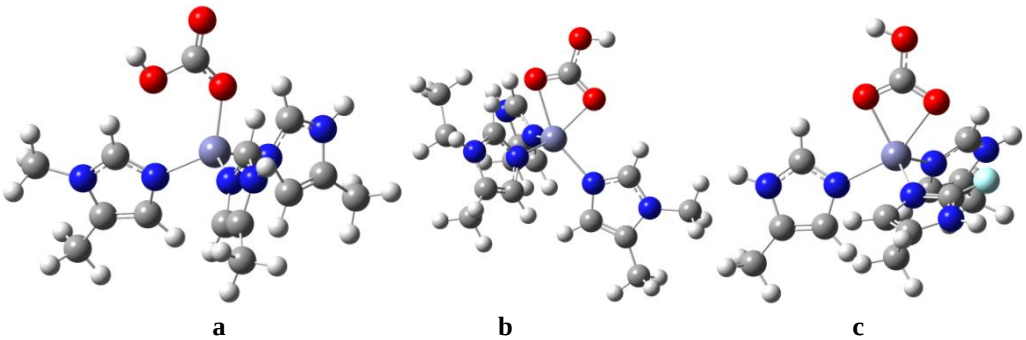

a **b** **c**

Fig.8. Optimized configuration of the CO_2 interaction with OH in various models a=model-1, b=model-9 and c=model-13

A close scrutiny of Fig. 8(a) shows that CO_2 interacts with the H on the OH in the model that migrates to the O of CO_2 to form HCO_3^- leading to a new coordination mode with Zn atom, mono-dentate in model 1 and bridge bi-dentate in models 9 & 13 respectively. This directly reflects in the binding energies. Model-1 has lower binding energy than model-13 and model-9. The Zn-O bond length in model-1 is 1.95 Å, and the average Zn-O bond length in model-9 and model-13 are 2.19 Å and 2.16 Å respectively. The order of stability of the HCO_3^- on these models is: 1<13<9. Although, the models 13 and 9 have similar type of coordination modes resembling that observed in pure model, with the small exception being that the H is on any one of the coordinated oxygens ie., on the free O of HCO_3^-. Hence, it is presumed that the newly obtained configurations may direct the reaction differently. Thus, the following mechanism is proposed in which after the interaction of CO_2 with OH^-, the HCO_3^- formed will be further taking up one H^+ to form *OCOHOH species on the active site. After optimization, the obtained configurations are presented in Fig.9.

Table 4. Structural parameters of H_2O on the modified model, natural bonding orbital charge on the atoms, Gibbs free energy of deprotonation and binding energy(B.E.) of CO_2

				NBO charges |q|			ΔG	CO_2
	O-H4	**O-H3**	**Zn-O**	**O**	**H3**	**H4**	**(eV)**	**B.E. (eV)**
1	0.97	0.97	2.13	-0.979	0.539	0.541	-7.96	-0.58
2	0.97	0.97	2.14	-0.978	0.539	0.539	-7.92	-0.25
3	0.97	0.97	2.14	-0.977	0.539	0.538	-7.84	-0.26
4	0.97	0.97	2.14	-0.979	0.540	0.539	-7.92	-0.25
5	0.97	0.97	2.14	-0.977	0.538	0.538	-7.83	-0.25
6	0.97	0.97	2.14	-0.975	0.537	0.538	-7.74	-0.24
7	0.97	0.97	2.14	-0.817	0.483	0.485	-7.84	-0.26
8	0.97	0.97	2.14	-0.977	0.540	0.538	-7.79	-0.34
9	0.97	0.97	2.14	-0.977	0.539	0.538	-7.88	-1.01
10	0.97	0.97	2.14	-0.977	0.538	0.538	-7.82	-0.23
11	0.97	0.97	2.13	-0.824	0.488	0.479	-7.96	-0.21
12	0.97	0.97	2.13	-0.827	0.479	0.488	-8.09	-0.24
13	0.97	0.97	2.13	-0.982	0.542	0.538	-8.06	-0.92
14	0.97	0.97	2.11	-0.823	0.489	0.482	-7.90	-0.27
15	0.97	0.97	2.11	-0.825	0.488	0.480	-7.98	-0.20
16	0.97	0.97	2.11	-0.824	0.488	0.482	-7.98	-0.09
17	0.97	0.97	2.11	-0.982	0.540	0.543	-7.98	-0.21
18	0.97	0.97	2.10	-0.986	0.543	0.541	-7.76	-0.49
19	0.97	0.97	2.09	-0.985	0.537	0.536	-7.83	-0.49
20	0.97	0.97	2.12	-0.980	0.542	0.542	-8.12	-0.19
21	0.97	0.97	2.11	-0.987	0.539	0.537	-8.10	-0.16
22	0.97	0.98	2.24	-0.967	0.519	0.529	-7.77	-0.28
23	0.97	0.97	2.11	-0.980	0.542	0.539	-7.76	-0.16
24	0.97	0.97	2.12	-0.984	0.544	0.543	-8.41	-0.22
25	0.97	0.97	2.13	-0.982	0.543	0.542	-8.25	-0.22
26	0.97	0.97	2.13	-0.981	0.542	0.541	-8.14	-0.22
27	0.97	0.97	2.12	-0.983	0.543	0.544	-8.26	-0.18

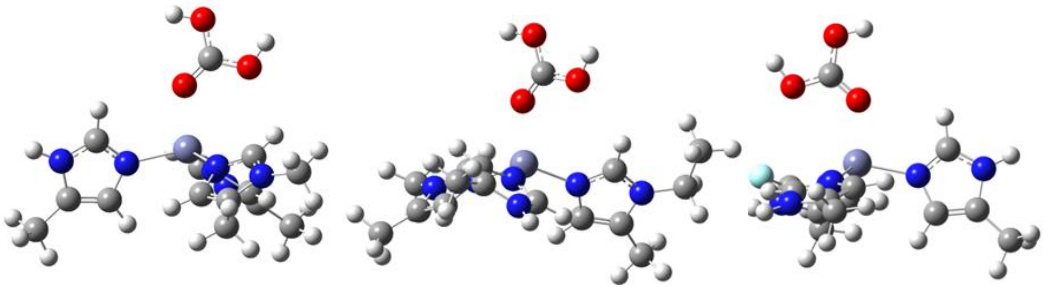

a **b** **c**

Fig.9. Optimized configuration of *OCOHOH species on model a-model-1, b-model-9 and c-model-13.

Fig. 9. reveals that even though, initially the coordination of HCOO may be different, after the uptake of H^+ the bond involved in the coordination gets cleaved before finally forming the H_2CO_3. The formed species then easily gets desorbed from the active site and seems to be simply held physically on. This result indicates that even in the new mode of CO_2 adsorption, it is finally converted easily into the H_2CO_3.

4. Conclusion

An attempt of mimicking the natural activity of carbonic anhydrase towards conversion of CO_2 into H_2CO_3 through simple models, was undertaken to elucidate its activity at DFT/B3LYP level. The results suggest that on the designed model, spontaneous activity could be observed in the original active site. Furthermore, this result supports the observed activity upon addition of ZIFs in photocatalytic reactions, since, the active sites easily capture and activate CO_2.

Acknowledgments

The authors thankful to Department of Science and Technology (DST), India, for setting up the National Centre for Catalysis Research (NCCR), and High Performance Computing Environment (HPCE), Indian Institute of Technology Madras (IITM) for supporting computational facilities. Further R. S. is thankful to Council of Scientific Industrial Research (CSIR) for fellowship., Ref.No. 08/117(0001)-2013-EMR-I.

References

[1] G. Centi, S. Perathoner, Opportunities and prospects in the chemical recycling of carbon dioxide to fuels, Catalysis Today, 148 (2009) 191-205.

[2] A.M. Appel, J.E. Bercaw, A.B. Bocarsly, H. Dobbek, D.L. DuBois, M. Dupuis, J.G. Ferry, E. Fujita, R. Hille, P.J.A. Kenis, C.A. Kerfeld, R.H. Morris, C.H.F. Peden, A.R. Portis, S.W. Ragsdale, T.B. Rauchfuss, J.N.H. Reek, L.C. Seefeldt, R.K. Thauer, G.L. Waldrop, Frontiers, Opportunities, and Challenges in Biochemical and Chemical Catalysis of CO_2 Fixation, Chemical Reviews, 113 (2013) 6621-6658.

[3] M. Aresta, A. Dibenedetto, Utilisation of CO_2 as a chemical feedstock: opportunities and challenges, Dalton transactions, 28 (2007) 2975-2992.

[4] S. Schenk, J. Notni, U. Kohn, K. Wermann, E. Anders, Carbon dioxide and related heterocumulenes at zinc and lithium cations: bioinspired reactions and principles, Dalton transactions, 35 (2006) 4191-4206.

[5] G. Parkin, Synthetic Analogues Relevant to the Structure and Function of Zinc Enzymes, Chemical Reviews, 104 (2004) 699-768.

[6] M. Raynal, P. Ballester, A. Vidal-Ferran, P.W.N.M. van Leeuwen, Supramolecular catalysis. Part 2: artificial enzyme mimics, Chemical Society reviews, 43 (2014) 1734-1787.

[7] T.R. Simmons, G. Berggren, M. Bacchi, M. Fontecave, V. Artero, Mimicking hydrogenases: From biomimetics to artificial enzymes, Coord. Chem. Rev., 270–271 (2014) 127-150.

[8] M.J. Wiester, P.A. Ulmann, C.A. Mirkin, Enzyme Mimics Based Upon Supramolecular Coordination Chemistry, Angewandte Chemie International Edition, 50 (2011) 114-137.

[9] C. Raksakoon, T. Maihom, M. Probst, J. Limtrakul, Hydration of Carbon Dioxide in

Copper-Alkoxide Functionalized Metal–Organic Frameworks: A DFT Study, The Journal of Physical Chemistry C, 119 (2015) 3564-3571.

[10] M. Verma, K.B. Sravan Kumar, P.A. Deshpande, Computational Insights into the Activity of Transition Metals for Biomimetic CO_2 Hydration, The Journal of Physical Chemistry C, 120 (2016) 5577-5584.

[11] G. Jin, C.G. Werncke, Y. Escudié, S. Sabo-Etienne, S. Bontemps, Iron-Catalyzed Reduction of CO_2 into Methylene: Formation of C–N, C–O, and C–C Bonds, Journal of the American Chemical Society, 137 (2015) 9563-9566.

[12] S. Bagherzadeh, N.P. Mankad, Catalyst Control of Selectivity in CO_2 Reduction Using a Tunable Heterobimetallic Effect, Journal of the American Chemical Society, 137 (2015) 10898-10901.

[13] C.C. Chong, R. Kinjo, Hydrophosphination of CO_2 and Subsequent Formate Transfer in the 1,3,2-Diazaphospholene-Catalyzed N-Formylation of Amines, Angewandte Chemie, 127 (2015) 12284-12288

[14] Q. Liu, Z.-X. Low, L. Li, A. Razmjou, K. Wang, J. Yao, H. Wang, ZIF-8/Zn_2GeO_4 nanorods with an enhanced CO_2 adsorption property in an aqueous medium for photocatalytic synthesis of liquid fuel, J. Mater. Chem. A., 1 (2013) 11563-11563.

[15] H.-P. Jing, C.-C. Wang, Y.-W. Zhang, P. Wang, R. Li, Photocatalytic degradation of methylene blue in ZIF-8, RSC Adv., 4 (2014) 54454-54462.

[16] S. Wang, W. Yao, J. Lin, Z. Ding, X. Wang, Cobalt Imidazolate Metal–Organic Frameworks Photosplit CO_2 under Mild Reaction Conditions, Angewandte Chemie International Edition, 53 (2014) 1034-1038.

[17] M.J. Frisch, G.W. Trucks, H.B. Schlegel, G.E. Scuseria, M.A. Robb, J.R. Cheeseman, G. Scalmani, V. Barone, B. Mennucci, G.A. Petersson, H. Nakatsuji, M. Caricato, X. Li, H.P. Hratchian, A.F. Izmaylov, J. Bloino, G. Zheng, J.L. Sonnenberg, M. Hada, M. Ehara, K. Toyota, R. Fukuda, J. Hasegawa, M. Ishida, T. Nakajima, Y. Honda, O. Kitao, H. Nakai, T. Vreven, J.A. Montgomery Jr., J.E. Peralta, F. Ogliaro, M.J. Bearpark, J. Heyd, E.N. Brothers, K.N. Kudin, V.N. Staroverov, R. Kobayashi, J. Normand, K. Raghavachari, A.P. Rendell, J.C. Burant, S.S. Iyengar, J. Tomasi, M. Cossi, N. Rega, N.J. Millam, M. Klene, J.E. Knox, J.B. Cross, V. Bakken, C. Adamo, J. Jaramillo, R. Gomperts, R.E. Stratmann, O. Yazyev, A.J. Austin, R. Cammi, C. Pomelli, J.W. Ochterski, R.L. Martin, K. Morokuma, V.G. Zakrzewski, G.A. Voth, P. Salvador, J.J. Dannenberg, S. Dapprich, A.D. Daniels, Ö. Farkas, J.B. Foresman, J.V. Ortiz, J. Cioslowski, D.J. Fox, Gaussian 09, Gaussian, Inc., Wallingford, CT, USA, 2009, Gaussian Revision C.01.

[18] F. Pannetier, G. Ohanessian, G. Frison, Comparison between [small alpha]- and [small beta]-carbonic anhydrases: can $Zn(His)_3(H_2O)$ and $Zn(His)(Cys).2(H_2O)$ sites lead to equivalent enzymes?, Dalton transactions, 40 (2011) 2696-2698.

Turkish Computational and Theoretical Chemistry

Turkish Comp Theo Chem (TC&TC)

Volume(Issue): 1(1) – Year: 2017 – Pages: 27-34

Received: 04.05.2017 ***Accepted:*** 07.05.2017 *Research Article*

5–Fluorouracil: Computational Studies of Tautomers and NMR Properties

Mahmoud Mirzaei[1]

[a]Bioinformatics Research Center, School of Pharmacy and Pharmaceutical Sciences, Isfahan University of Medical Sciences, Isfahan, Iran

Abstract: Chemical computations were performed to investigate stabilities and properties for tautomers of 5–fluorouracil (5FU). In addition to optimized properties, nuclear magnetic resonance (NMR) parameters were calculated for all atoms of the stabilized structures. Di–keto form of 5FU is the most stable structure and keto–enol and di–enol structural forms are tautomeric structures. According to the results, the polar and non-polar solvents media and tautomeric forms are both important in characterizing 5FU structures.

Keywords: *5–Fluorouracil; Tautomer; Chemical computations; Density functional theory; Chemical shift.*

1. Introduction

5–Flourouracil (5FU), as an anticancer drug, is a fluorinated derivative of uracil nucleobase with the fluorination of carbon number five of pyrimidine ring [1]. 5FU has been used for therapies of several types of cancers for years; however, the side effects are still a considerable problem for this popular anticancer drug [2, 3]. Formations of tautomeric structures commonly for heterocyclic structures could be one of the reasons for appearing the side effects [4]. Tautomers are formed by the exchange of hydrogen atoms between nitrogen and oxygen atoms of the heterocyclic ring making high energetic unstable structures ready to destroy the neighborhood systems [5, 6]. Tautomers are also origins of mutations in genetics yielding several defects to living systems [7]. Considerable efforts have been dedicated to characterize and identify various aspects of tautomers especially for biological related counterparts up to now [8 – 11]. Computations are one of the proper techniques for systematic investigations of stabilities and properties for tautomeric systems at the atomic and molecular scales [12]. Characterizations of tautomers of 5FU and other uracil derivatives are interesting for the scientists due to their importance in the living systems [13 – 16]. Within this work, we have performed quantum chemical computations to investigate the stabilities and nuclear magnetic resonance (NMR) properties of tautomers of 5FU in different solvent systems. According to the results of earlier works, 5FU could participate in tautomerization process similar to uracil nucleobase, in which the di–keto form is the most stable structure. Tautomers could be in keto–enol and di–enol forms according to the exchange of hydrogen positions between nitrogen and oxygen atoms. Although the di–keto form has been seen as the most stable one, but the existence of keto–enol and di–enol tautomers are still possible (Fig. 1) [17]. Chemical environments could employ effects on the initial properties of matters especially presence of hydrophobic or hydrophilic solvents. Hereby, effects of five solvents including water, methanol, ethanol, chloroform, and carbon

[1] Corresponding Author

e-mail: mdmirzaei@pharm.mui.ac.ir

tetrachloride have been investigated on the properties of 5FU and its tautomers within current research. In fact, the major question of this work is to investigate the properties of 5FU and tautomers in the conventional and mostly used solvent media.

2. Computational Details

Density functional theory (DFT) calculations have been performed employing the B3LYP exchange–correlation functional and the 6–31G* standard basis set as implemented in the Gaussian 98 package [18]. First, the investigated molecular structures of 5FU including di–keto (Fig. 1, Panel a), keto–enol (Fig. 1, Panels b – e), and di–enol (Fig. 1, Panel f), totally six forms, have been optimized to achieve the optimized structures corresponding to minimum energies. Next, the presence of five conventional and mostly used solvents including water (H2O), methanol (MeOH), ethanol (EtOH), chloroform (CHCl3), and carbon tetrachloride (CCl4) have been considered in the calculations of atomic and molecular properties. The molecular properties including total energies, dipole moments, and energies for the highest occupied and the lowest unoccupied molecular orbitals (HOMO and LUMO) have been evaluated in different solvent systems (Table 1). Furthermore, chemical shielding (σiso) tensors have been calculated for the atoms of optimized structures based on the gauge–included atomic orbital (GIAO) approach [19] and they have been converted to chemical shifts (δ /ppm) using equation of $\delta = \sigma_{iso,\,reference} - \sigma_{iso,\,sample}$ (Tables 2 – 6). To obtain magnitudes of σiso, reference , tetramethylsilane (TMS) has been used for C and H atoms, ammonia (NH3) has been used for N atoms, and water (H2O) has been used for O atoms, details of evaluations are described elsewhere [20]. Nuclear magnetic resonance (NMR) spectroscopy is among the most versatile techniques to investigate the properties of matters especially in living systems [21]. Chemical shielding tensors are originated from the electronic sites of atoms capable of detecting any perturbations employed to these sites. It is worth noting that, the molecular properties (Table 1) are not enough to recognize the characteristics of matters whereas NMR properties could reveal insightful information at the atomic scale to better achieve the purpose [22, 23]. Due to the complexity of experiments, computations could predict or interpret the characteristics of matters, especially for unstable tautomeric structures. The combinations of results of molecular (Table 1) and atomic (Tables 2 – 6) parameters could very well describe the properties of investigated 5FU models (Fig. 1).

3. Results and Discussion

The models of this work include various forms of 5FU including the initial di–keto form and the keto–enol and di–enol tautomers (Fig. 1). For a quick description of models, nitrogen atoms numbers one and three have their original hydrogen atoms in the initial di–keto form (Panel a, Fig. 1). To make the tautomers, first the position of hydrogen atom number one has been exchanged to oxygen atom number two then atom number four to make the keto–enol forms (Panels b and c, Fig. 1). Afterwards, the hydrogen atom number three has been exchanged to oxygen atom number two then atom number four to make the second set of keto–enol forms (Panels d and e, Fig. 1). For the di–enol form (Panel f, Fig. 1), both of hydrogen atoms have been exchanged to oxygen atoms to make the third set of tautomers for the investigated 5FU.

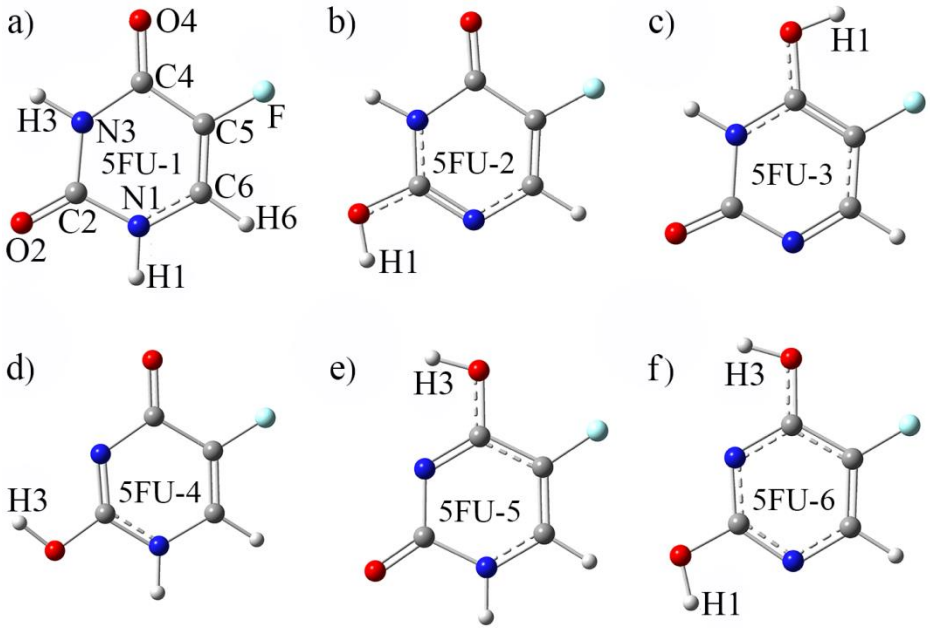

Figure 1. (a) Di–keto, (b) – (e) keto–enol, and (f) di–enol forms of 5FU

The optimization processes indicated that the magnitudes of energies for di–keto forms of 5FU are smaller than other tautomeric forms among different solvents, which shows the best stability of this structure among available tautomers (Table 1). However, the results show that the differences between the energy magnitudes are not significant, which is a clue for participation of the initial di–keto form in the tautomerization processes without a major energy barrier. The results indicate that the polarities of tautomers are changed in different solvents as indicated by dipole moments. It is known that the electronic properties of matters could detect different electrical effects employed by solvents media. 5FU–4 and 5FU–6 have respectively the largest and the smallest magnitudes of dipole moments in all solvent systems. Comparing the effects of solvents reveals that the structures in H2O solvent have the largest magnitude of dipole moments whereas the magnitudes in CCl4 solvents are the smallest ones. The trends of dipole moments properties could be explained because of different charge distributions in each of tautomers and solvents. The energies for the highest occupied and the lowest unoccupied molecular orbitals (HOMO and LUMO) also demonstrate that the conducting properties of structures are changed among the investigated tautomers and solvents. The HOMO and LUMO properties are important for several electronic characteristics of matters especially towards other matters. Moreover, the electronic properties could define the reactivity of chemical substances, which are important to define their characteristic roles in chemical or biochemical systems. The exact energy levels of HOMO and LUMO and the magnitudes of differences between the two levels are mainly due to changes happened to initial properties of matters. It is noted that the di–keto form (5FU–1) is the evidence for tracking the changes of other structures among the models of this work. As an overview of this section, it could be mentioned that the molecular properties of tautomers are different from the evidence molecule.

Table 1. Optimized properties*

Atom	Solvent	5FU–1	5FU–2	5FU–3	5FU–4	5FU–5	5FU–6
E_{Total} /keV	H_2O	–13.988	–13.987	–13.987	–13.987	–13.987	–13.987
	MeOH	–13.988	–13.987	–13.987	–13.987	–13.987	–13.987
	EtOH	–13.988	–13.987	–13.987	–13.987	–13.987	–13.987
	$CHCl_3$	–13.988	–13.987	–13.987	–13.987	–13.987	–13.987
	CCl_4	–13.988	–13.987	–13.987	–13.987	–13.987	–13.987
D_{Moment} /Debye	H_2O	5.056	5.123	7.528	8.798	4.589	0.647
	MeOH	5.021	5.093	7.475	8.732	4.554	0.644
	EtOH	5.002	5.077	7.447	8.697	4.537	0.642
	$CHCl_3$	4.705	4.826	7.009	8.149	4.252	0.620
	CCl_4	4.391	4.548	6.541	7.568	3.949	0.603
E_{HOMO} /eV	H_2O	–6.593	–6.483	–6.332	–6.630	–6.492	–6.739
	MeOH	–6.598	–6.483	–6.333	–6.629	–6.493	–6.739
	EtOH	–6.601	–6.483	–6.334	–6.629	–6.494	–6.739
	$CHCl_3$	–6.647	–6.485	–6.340	–6.628	–6.502	–6.737
	CCl_4	–6.698	–6.487	–6.347	–6.624	–6.509	–6.734
E_{LUMO} /eV	H_2O	–1.185	–1.138	–1.468	–0.869	–1.347	–1.073
	MeOH	–1.191	–1.139	–1.471	–0.870	–1.352	–1.074
	EtOH	–1.194	–1.140	–1.472	–0.869	–1.354	–1.074
	$CHCl_3$	–1.239	–1.152	–1.498	–0.869	–1.393	–1.077
	CCl_4	–1.289	–1.165	–1.528	–0.869	–1.435	–1.080

* See Fig. 1 for the model structures.

Moreover, the polarities as detected by the magnitudes of dipole moments are also different for the investigated structures among the tautomeric forms and solvents media. Although the stabilities are not very different, but the type of solvent has a remarkable effect on the initial properties of 5FU model structures. The molecular orbital energy levels and their corresponding electronic properties are mainly dependent on tautomeric forms and solvents media.

NMR Properties

To better investigate the considered systems at the atomic levels, chemical shifts (δ /ppm) for atoms of the optimized 5FU structures are listed in Tables 2 – 6 based on the atoms types in NMR measurements. The first set of NMR data belongs to three hydrogen atoms of 5FU in different solvents (Table 2). Hydrogen atoms numbers one and three (H1 and H3) participate in tautomerization processes but hydrogen atom number six (H6) is kept fixed. Interestingly, the properties for H6 are changed in tautomeric structures meaning that in–direct effects detection of tautomerization by the electronic site of this atom. For H1, which is in its original position in 5FU–1, 5FU–4, and 5FU–5, different results are seen. When the position of H3 is changed, the effects of tautomerization on the properties of this atom are still recognized. For H3, which is in its original position in 5FU–1, 5FU–2, and 5FU–3, different results are also achieved parallel to results of H1. Indeed, the hydrogen atom plays the major role in tautomerization process, in which its own properties are changed among tautomeric structures. Moreover, the largest magnitudes of shifts are seen in H2O solvent and the smallest magnitudes are seen for the CCl4 solvent. In fact, the hydrogen atom has a small magnitude of electron at the atomic site but it is still enough to detect the effects of any employed perturbations revealing the importance of NMR properties in materials characterizations.

The NMR properties for four carbon atoms are listed in Table 3. Since the carbon atoms make the skeleton of heterocyclic ring, their properties are very important in definitions of their structural properties. Changes of the hydrogen atom position around the ring could make effects to the initial properties of carbon atoms.Different magnitudes of

shifts for each of carbon atoms in different tautomers and solvents show that the properties are very sensitive to environment. Although C5 and C6 do not directly participate in tautomerization, but the results indicate that the properties are changed during this process. Polarities of solvents are also important for the properties of carbon atoms as could be seen by the changes of chemical shifts in different environments.

Table 2. ^{1}H Chemical shifts (δ /ppm)*

Atom	Solvent	5FU–1	5FU–2	5FU–3	5FU–4	5FU–5	5FU–6
H_1	H_2O	5.876	5.636	5.839	6.552	6.595	5.808
	MeOH	5.852	5.619	5.814	6.519	6.572	5.795
	EtOH	5.839	5.610	5.801	6.502	6.560	5.788
	$CHCl_3$	5.630	5.464	5.587	6.227	6.366	5.674
	CCl_4	5.398	5.292	5.350	5.931	6.152	5.544
H_3	H_2O	6.370	7.308	6.750	5.340	5.750	5.635
	MeOH	6.364	7.295	6.731	5.328	5.741	5.622
	EtOH	6.360	7.288	6.722	5.321	5.736	5.614
	$CHCl_3$	6.302	7.171	6.561	5.207	5.652	5.493
	CCl_4	6.225	7.036	6.379	5.064	5.542	5.350
H_6	H_2O	6.946	7.318	8.201	6.870	7.208	7.841
	MeOH	6.929	7.311	8.201	6.850	7.192	7.835
	EtOH	6.920	7.308	8.201	6.839	7.184	7.833
	$CHCl_3$	6.780	7.248	8.199	6.672	7.047	7.788
	CCl_4	6.627	7.181	8.190	6.492	6.898	7.739

* See Fig. 1 for the model structures.

Table 3. ^{13}C Chemical shifts (δ /ppm)*

Atom	Solvent	5FU–1	5FU–2	5FU–3	5FU–4	5FU–5	5FU–6
C_2	H_2O	138.112	144.356	142.311	144.616	142.258	152.386
	MeOH	138.072	144.310	142.249	144.553	142.196	152.388
	EtOH	142.249	144.286	142.160	144.519	142.163	152.388
	$CHCl_3$	137.713	143.886	141.682	143.976	141.625	152.393
	CCl_4	137.328	143.433	141.085	143.365	141.020	152.386
C_4	H_2O	148.562	145.648	145.639	154.594	154.088	151.672
	MeOH	148.509	145.594	145.562	154.513	154.083	151.668
	EtOH	145.562	145.566	145.522	154.470	154.080	151.666
	$CHCl_3$	148.037	145.109	144.883	153.785	154.016	151.619
	CCl_4	147.553	144.602	144.210	153.026	153.905	151.546
C_5	H_2O	136.181	142.429	128.608	142.174	129.569	136.239
	MeOH	136.202	142.456	128.536	142.214	129.555	236.229
	EtOH	128.536	142.471	128.498	142.236	129.547	136.225
	$CHCl_3$	136.390	142.710	127.909	142.581	129.431	136.154
	CCl_4	136.582	142.980	127.310	142.959	129.313	136.086
C_6	H_2O	121.671	133.101	148.045	117.887	126.850	140.538
	MeOH	121.528	133.039	148.054	117.695	126.721	140.504
	EtOH	148.054	133.008	148.058	117.594	126.653	140.486
	$CHCl_3$	120.275	132.492	148.091	116.025	125.592	140.204
	CCl_4	119.040	131.926	148.053	114.406	124.490	139.912

* See Fig. 1 for the model structures.

Table 4. ^{15}N Chemical shifts (δ /ppm)*

Atom	Solvent	5FU–1	5FU–2	5FU–3	5FU–4	5FU–5	5FU–6
N_1	H_2O	120.616	185.498	247.807	110.656	142.896	228.624
	MeOH	120.398	185.482	248.454	110.329	142.7007	228.685
	EtOH	120.284	185.474	248.793	110.159	142.599	228.718
	$CHCl_3$	118.493	185.369	254.214	107.496	141.003	229.280
	CCl_4	116.622	185.314	249.905	104.745	139.356	229.979
N_3	H_2O	157.261	153.487	141.543	214.289	218.059	211.600
	MeOH	157.233	153.405	141.370	214.492	218.341	211.719
	EtOH	157.218	153.362	141.279	214.598	218.489	211.781
	$CHCl_3$	156.966	152.671	139.844	216.255	220.826	212.752
	CCl_4	156.670	151.911	138.318	217.969	223.303	213.768

* See Fig. 1 for the model structures.

Table 5. ^{17}O Chemical shifts (δ /ppm)*

Atom	Solvent	5FU–1	5FU–2	5FU–3	5FU–4	5FU–5	5FU–6
O_2	H_2O	265.784	123.014	289.433	123.430	282.438	130.720
	MeOH	266.368	122.931	290.613	123.308	283.495	130.845
	EtOH	266.675	122.888	291.234	123.245	284.052	130.909
	$CHCl_3$	271.707	122.183	301.344	122.251	293.154	131.952
	CCl_4	277.430	121.416	312.666	121.228	303.443	133.079
O_4	H_2O	298.320	307.439	99.897	274.180	134.099	120.311
	MeOH	297.095	308.440	99.658	272.196	134.178	120.378
	EtOH	296.452	308.966	99.534	271.153	134.219	120.413
	$CHCl_3$	286.201	315.708	97.592	254.416	134.810	120.936
	CCl_4	275.097	306.338	95.601	236.075	135.316	121.443

* See Fig. 1 for the model structures.

The magnitudes of chemical shifts of nitrogen atoms (Table 4) are significantly changed from the initial di–keto form to keto–enol and di–enol forms. The solvent effects are also observed for the NMR properties of nitrogen atoms.

O2 and O4 are two different types of oxygen atoms, a urea type and an amide type, respectively. The magnitudes of chemical shifts for O2 and O4 (Table 5) also demonstrate different chemical properties for these atoms according to their own types. The keto and enol forms (oxo and hydroxy forms) are very important to be considered for each oxygen atom. The oxygen atoms are also similar to nitrogen atoms due to excess of electrons in the valance shells; therefore, the effects are significant on their properties. The fluorine atom, which is the characteristic atom of 5FU, also shows the detections of effects through tautomerization. The major effects are especially seen for 5FU–3, in which the hydrogen atom has been oriented to fluorine atom. The effects of solvents on the properties of fluorine atom are also observed. As an overview of atomic scale NMR properties, it could be mentioned that the properties of all atoms could undergo significant effects through tautomerization processes, in which the type of solvent media and the form of tautomeric structure are both important for chemical characterizations. From H_2O to CCl_4, polar to non-polar solvents, the influences are detected by the NMR properties of atoms. Since the electrical properties of solvents are different, the corresponding electronic properties are also different for atoms in different solvent media. It could be mentioned that the NMR properties, which are originated from the electronic sites, could well detect the atomic scale properties of 5FU tautomers in different media. The potential reader can find here that choosing the solvent media is very important for chemical substances characterizations especially at the atomic levels.

4. Conclusion

The performed quantum chemical computations on the possible forms of 5FU during tautomerization could reveal some remarkable trends. First, the molecular properties are not good enough to well describe the characteristics of matters and the atomic scale properties are needed for the purpose. Second, the small magnitudes of energy differences among the initial di–keto form and the keto–enol and di–enol forms indicated that the tautomeric structures of 5FU could be formed without any significant energy barriers. Third, the type of solvent media and the type of tautomeric could influence on the properties of 5FU structures as indicated by the magnitudes of dipole moments and HOMO / LUMO properties. Fourth, atomic scale NMR properties could well describe the electronic properties of 5FU structures as indicated by the magnitudes of chemical shifts in different tautomers and solvents media. And finally, due to specific electrical properties for each solvent, it is important to select the type of solvent for the studies. Polar solvents like H2O, MeOH and EtOH are almost similar but there are significant differences between the polar solvents and the non-polar solvents, $CHCl_3$ and CCl_4; therefore, the solvent shod be carefully chosen for the desired investigations.

References

[1] L. Fallon, The crystal and molecular structure of 5-fluorouracil, Acta Crystallographica Section B 29 (1973) 2549–2556.

[2] A. González-Sarrías, J. Tomé-Carneiro, A. Bellesia, F.A. Tomás-Barberán, J.C. Espín, The ellagic acid-derived gut microbiota metabolite, urolithin A, potentiates the anticancer effects of 5-fluorouracil chemotherapy on human colon cancer cells, Food & Function 6 (2015) 1460–1469.

[3] S.S. Saneeymehri, K.R. Markey, A. Mahipal, Paradoxical effect of capecitabine in 5-fluorouracil-induced cardiotoxicity: A case vignette and literature review, Journal of Oncology Pharmacy Practice 22 (2016) 552-555.

[4] M. Malińska, P. Krzeczyński, E. Czerniec-Michalik, K. Trzcińska, P. Cmoch, A. Kutner, K. Woźniak, Crystal structure and tautomerism of capecitabine, Journal of Pharmaceutical Sciences 103 (2014) 587–593.

[5] T. Lukmanov, S.P. Ivanov, E.M. Khamitov, S.L. Khursan, Relative stability of keto-enol tautomers in 5, 6-substituted uracils: Ab initio, DFT and PCM study, Computational and Theoretical Chemistry 1023 (2013) 38–45.

[6] M. Monajjemi, B. Honarparvar, H. Monajemi, Investigation of NQR parameters on the tetrazole-azide tautomeric equilibria: a DFT study, Journal of the Mexican Chemical Society 50 (2006) 143–148.

[7] N.R. Jena, A.E. Mark, P.C. Mishra, Does tautomerization of FapyG influence its mutagenicity?, Chemphyschem 15 (2014) 1779–1784.

[8] D. Gur, L.J. Shimon, Crystal structure of disodium 2-amino-6-oxo-6, 7-dihydro-1H-purine-1, 7-diide heptahydrate, Acta Crystallographica E 71 (2015) 281–283.

[9] M. Mirzaei, H.R. Kalhor, N.L. Hadipour, Covalent hybridization of CNT by thymine and uracil: A computational study, Journal of Molecular Modeling 17 (2011) 695–699.

[10] N. Markova, V. Enchev, I. Timtcheva, Oxo−hydroxy tautomerism of 5-fluorouracil: Water-assisted proton transfer, The Journal of Physical Chemistry A 109 (2005) 1981–1988.

[11] T. Marino, N. Russo, M. Toscano, Density functional study of oxo-hydroxy tautomerism of 5-fluorouracil, International Journal of Quantum Chemistry 62 (1997) 489–494.

[12] X. Guo, Y. Zhao, Z. Cao, Ab initio study on ultrafast excited-state decay of allopurinol keto-N9H tautomer from gas phase to aqueous solution. The Journal of Physical Chemistry A 118 (2014) 9013–9020.

[13] S. Ortiz, M.A. Palafox, V.K. Rastogi, T. Akitsu, I.H. Joe, S. Kumar, Simulation of a tetramer form of 5-chlorouracil: The vibrational spectra and molecular structure in the isolated and in the solid state by using DFT calculations, Spectrochimica Acta Part A 110 (2013) 404-418.

[14] T.M. El-Gogary, A.M. El-Nahas, Origin of reverse stability of diphosphouracil tautomers compared to their analogue uracil: DFT and ab initio study, Journal of Molecular Structure: THEOCHEM 851 (2008) 54–62.

[15] A.F. Jalbout, B. Trzaskowski, Y. Xia, Y. Li, X. Hu, H. Li, A. El-Nahas, L. Adamowicz, Structures, stabilities and tautomerizations of uracil and diphosphouracil tautomers, Chemical Physics 332 (2007) 152–161.

[16] A. Buda, A. Syguła, MNDO study of the tautomers of nucleic bases: Part I. Uracil, thymine and cytosine, Journal of Molecular Structure: THEOCHEM 92 (1983) 255–265.

[17] M.J. Scanlan, I.H. Hillier, Accurate prediction of the relative energies of the six tautomers of uracil, Chemical Physics Letters 98 (1983) 545–547.

[18] M.J. Frisch, G.W. Trucks, H.B. Schlegel, G.E. Scuseria, M.A. Robb, et al., Gaussian 98 Revision A.7, Gaussian Inc., Pittsburgh, PA, 1998.

[19] S.K. Wolff, T. Ziegler, Calculation of DFT-GIAO NMR shifts with the inclusion of spin-orbit coupling, The Journal of Chemical Physics 109 (1998) 895–905.

[20] M. Mirzaei, N.L. Hadipour, Study of hydrogen bonds in 1-methyluracil by DFT calculations of oxygen, nitrogen, and hydrogen quadrupole coupling constants and isotropic chemical shifts, Chemical Physics Letters 438 (2007) 304–307.

[21] R.S. Drago, Physical Methods for Chemists. Saunders College Publishing, 2nd Ed., New York, 1992.

[22] M. Mirzaei, N.L. Hadipour, An investigation of hydrogen-bonding effects on the nitrogen and hydrogen electric field gradient and chemical shielding tensors in the 9-methyladenine real crystalline structure: A density functional theory study, The Journal of Physical Chemistry A 110 (2006) 4833–4838.

[23] M. Rafiee, M. Javaheri, A theoretical study of benzaldehyde derivatives as tyrosinase inhibitors using Ab initio calculated NQCC parameters, Molecular Biology Research Communications 4 (2015) 151–159.

Turkish Computational and Theoretical Chemistry

Turkish Comp Theo Chem (TC&TC)

Volume(Issue): 1(1) – Year: 2017 – Pages: 35-41

Received: 05.05.2017 ***Accepted:*** 22.05.2017 *Research Article*

Metal-mediated thymine base pair complexes: A DFT study

Ayhan ÜNGÖRDÜ [1], Nurten TEZER

Cumhuriyet University, Science Faculty, Chemistry Department, 58140 Sivas / Turkey

Abstract: The most stable of thymine-metal-thymine complexes and their geometries were determined. Method was used density functional theory, B3LYP. The calculations of systems containing C, H, N, O were described by the standard 6–311++G(d,p) basis set and LANL2DZ basis set were used for transition metals. Egap energy values of complexes were calculated by Chemissian program. Conductivity of metal-mediated thymine base pair complexes were predicted. In nanoworld, this study is expected to be shown the way for future practical applications.

Keywords: *metal-DNA; conductivity; nanowires; DFT calculations.*

1. Introduction

Nucleic acids, linked chains purine (adenine and guanine) and pyrimidine (uracil, thymine and cytosine) bases carries the genetic information in living systems. Recently, there have been many studies to explain the properties of the nucleic acids in nonbiological contexts. Some properties of nucleic acids enable them to be used to produce the nanostructures (nanomaterials, nanowires…) [1]. One of the properties of the nucleic acids is to form metal-DNAs. Metal-DNAs may be obtained by treatment with double-stranded DNA of the metal cation [2]. Alkali (or rare-earth) cations form only electrostatic interactions with the nucleobases [3,4], but transition metal cations are expected to interact with the nucleobases also by chemical bonding [5-10]. Additionally, transition metals have many functions in the nanoworld. Due to the unique physical and chemical properties related to electronic conductivity of metal ions, they are involved in nucleic acids to form metal-mediated DNA bases [11]. DNA-based nanostructures can be formed in this way. DNA-based nanostructures attract attention because of their unique electrical, optical biological applications. The production of metal-DNA provides substantial benefits for their potential application as nanomagnets [12,13], as nanowires or as catalysts in chemical reactions.

Recently, metal-DNA have attracted much interest for the possibility of using such molecules as building blocks for electronic nano-devices [14-17]. If natural DNA would be a superior conductor for electrons and functional building blocks such as molecular transistors could be incorporated into DNA strands by chemical synthesis, it would be possible to construct the first generation of electronic circuits today (Fig. 1).

1.1. Metal-mediated thymine base pairs

The simplest pyrimidine base is thymine. It has become an important subject of theoretical or experimental work due to the biochemical importance [18,19]. It has been reported that natural thymine bases form metal-DNA. Two thymine (T–T) bases selectively capture mercury(II) cations and T-Hg-T complex forms. This complex occurs easily with mercury(II) cations [20-23]. T-Hg-T complex is

[1] Corresponding Author

e-mail: aungordu@cumhuriyet.edu.tr

formed by displacement of metal-base bond with hydrogen bond in natural DNA and they are also mismatched (Fig. 2) [24].

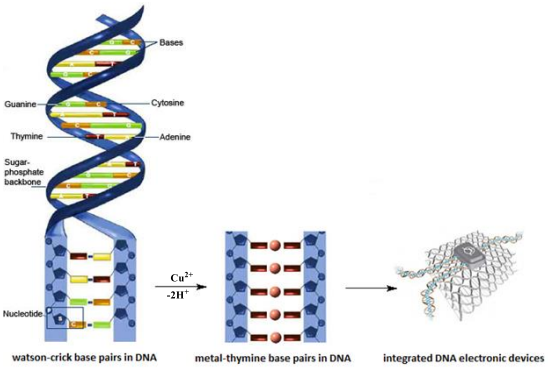

Fig. 1. The use of metal-DNA as conductive wires in nanotechnology.

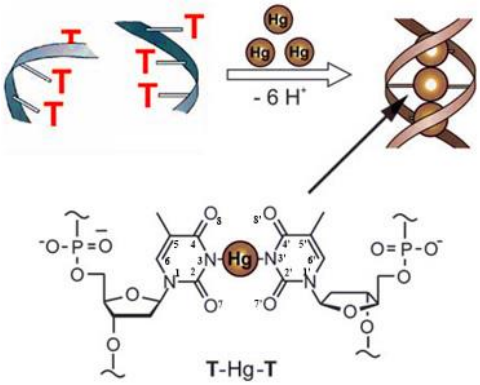

Fig. 2. Formation of T-Hg-T complex from upon addition of Hg^{2+} ions [20].

Studies from a number of groups have shown that mercury(II) ion binds to the nitrogen atoms between T–T mismatches (Fig. 2). One of them is Ono group. This group has found strong evidence for the structure of T–Hg–T by N15-NMR spectroscopy. ESI-MS spectroscopy has determined that up to five mercury(II) ions can stack between T-T bases (similarly to Fig. 1) [20,21].

After many studies in this area, it is known that the transition metal ion binding sites on the thymine consists primarily of the deprotonated nitrogen atoms (N3) and the oxygen positions (O7 or O8), depending on the coordinating metal [25-27]. Therefore, deprotonated thymine can be considered as bidentate ligand. Two main coordination geometries are expected for two bidentate ligands around a central metal ion: square planar and tetrahedral [24].

At high pH conditions, divalent metal cations (Zn^{2+}, Ni^{2+} and Co^{2+}) were reported by the Lee group to form complexes with unmodified DNA [28]. Upon adding these metal ions to DNA at pH 8.5, a pH decreases and NMR results were consistent with replacement of the imino proton (at N3) in each base pair of the duplex by a metal ion. Such metal–DNA complexes can be more conductive than DNA, with potential for the development of molecular wires and useful nanotechnological applications [28-30]. However, the exact structure and the electronic properties of metal-DNA are still controversial [31,32]. For instance, AFM study of metal-DNA duplexes showed that they have a very condensed structure compared to DNA duplexes that has yet to be explained [31].

The main goal of this work is to unravel conductivity of metal-mediated thymine base pairs for some divalent transition metal ions. We present and discuss the results of a DFT study of several metal-mediated T–Mn^{+}–T complexes (M = Hg, Cd, Zn, Cu, Ni, Pd, Pt and n = 2) in the gas phase. We find that all of the examined metal species are capable of binding Thymine–Thymine (T-T) base pairs in the ratio 1:2, and the resulting T–Mn^{+}–T base pairs have a low band gap. Using band gap, we determine the metal-DNA complex that creates the suitable conductor wire. These complexes are considered to be useful for nanotechnological applications.

2. Computational Details

Metal-mediated thymine base pair complexes were investigated by means of density functional theory (DFT) calculations. Because previous theoretical calculations shown that the B3LYP approach was cost-effective for studying transition metal-ligand systems [33]. The calculations of systems containing C, H, N, O were described by the standard 6–311++G(d,p) basis set [34]. For transition metals (Hg, Cd, Zn, Cu, Ni, Pd and Pt), LANL2DZ basis set was used [35] and Hg, Cd, Zn, Cu, Ni, Pd and Pt were described by the effective core potential (ECP) of Wadt and Hay pseudopotential [36,35b] with a doublet–ζ valence using the LANL2DZ. All of the systems were optimized at the B3LYP method. In all cases, the steady–state nature of the optimized metal-mediated thymine base pair complexes were confirmed by calculating the corresponding frequencies at the same computational level. For the

optimized geometries, the correlation energies were calculated by B3LYP density functional theory. The calculations were performed by using the GAUSSIAN 09-Revision D.01 package program [36]. The input files of mentioned complex were prepared with GaussView 5.0.8 program [37]. Closed-shell calculations were performed using the restricted formalism and open-shell calculations were performed using the unrestricted formalism (for Cu^{2+}). The energy difference (Egap) between HOMO and LUMO were calculated by using the Chemissian, version 4.43 demo program [38] (created in Chemissian based on Gaussian 09 calculations). The energy gaps were given as follows.

$$Egap = E_{LUMO} - E_{HOMO}$$

The band theory is related to molecular orbital theory [39]. In molecular orbital theory, while the highest occupied molecular orbital is called HOMO, the lowest unoccupied molecular orbital is called LUMO. The valence band (VB) represents HOMO and the conduction band (CB) represents LUMO [40]. The gap between the HOMO and LUMO level is called band gap or energy gap (Egap). The conductivity of metal-DNA can be examined by energy gap (Fig. 3).

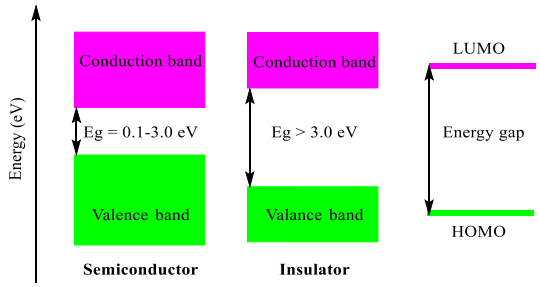

Fig. 3. The correlation between energy band diagram and HOMO-LUMO [39].

3. Results and Discussion

Thymine have an acidic imine proton. Therefore, imine proton is lost in the basic medium. Deprotonated thymine is formed as following:

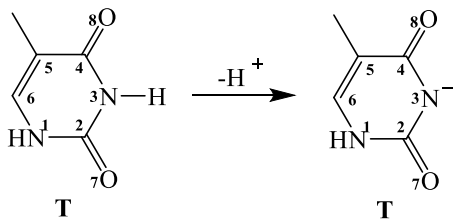

Metal-mediated thymine base pair complex can occur that metal cation react with deprotonated thymine anion. Formation of this reaction can show as in Fig. 4. As shown in the above reaction, metal cation (M^{2+}) binds from the region of deprotonated thymine anion (T^{-}) where the electron density is very (red area). Possible binding structures of Cu-mediated thymine base pairs is represented as in Fig. 5.

For these structures, relative energy values are given in Table 2. Considering the relative energy values, it is seen that the most stable structure is III structure. This can be explained as follows: Electronegative N atom at 1 position 1 of deprotonated thymine, by inductive effect, decreases the electron density of N3-O7 region of ligand. On the other hand, this cannot be said for N3-O8 region of ligand. Therefore, electron density of N3-O8 region is more than that of N3-O7 region. When metal binds from this region, the most stable complexes form. This is true for all complexes.

We have performed the calculations of ΔG and the results, at 298 K are reported in Table 3. We here define the complex formation energy by following formula:

$$\Delta G_{form.} = G_{T-M-T} - (2G_{T^-} + G_{M^{2+}})$$

Table 2. Relative energies (kcal.mol^{-1}) of three possible Cu-mediated thymine base pair complexes

Method	I	II	III
B3LYP/G-311++(d,p)-LANL2DZ (Cu)	0	-1,23	-6,28

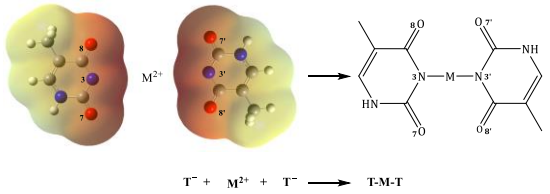

Fig. 4. The reaction pathway for metal mediated thymine base pair complexes

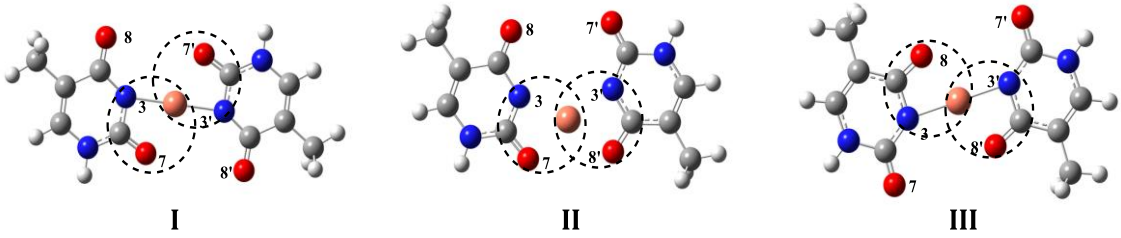

Fig. 5. Three possible binding structure for Cu-mediated thymine base pairs complex

It is seen from Table 3 that the studied complexes can be synthesized with reaction metal cation (M^{2+}) and deprotonated thymine anion (T^{-}) if required conditions provide (such as pH). Also, it is found that the especially planar complexes are more stable (~100 kcal/mol) than the non-planar complexes. Table 3 represents the complex formation energy, ΔG_{form}, which ranges from -525 kcal mol^{-1} (for Cd^{2+}) to -679 kcal mol^{-1} (for Pt^{2+}). The T-Pt-T is the most stable complex among all metal complexes.

A different look at the role of the metal moiety in the electronic structure of metallated base pairs can be given by inspecting the electron energy levels and the HOMO-LUMO gaps. In all of the computed T-M-T pairs the Egap changes by depending on the complex coordination. The energy gap change is an important metal-induced effect in view of nanotechnology applications. M-DNA's conductivity mechanism by electronic means is not yet fully elucidated [42]. One of the theoretical approach to explain the electrical conductivity is the band theory. In this work, the electrical conductivity of the T-M-T complexes have also tried to explain the band theory. For this, the frontier orbital energy levels for the most stable structures of metal complexes are found and the energy gaps (Egap) are determined. Egap values are calculated using the difference HOMO-LUMO values. We can divide into double-electron (closed-shell) and single-electron (open-shell) systems of examined complex structures. Except Cu^{2+}, studied other metal cation systems are closed-shell.

Table 3. Complex formation energies of T-M-T complexes (at 298,15 K)

Metal type	**G(Thymine anion)/a.u.**	**G (Metal cation/a.u.**	**G (Complex)/a.u.**	**ΔG(Complex)/kcal mol^{-1}**
Hg(II)	-453,644	-41,811	-949,942	**-529**
Cd(II)	-453,644	-47,173	-955,297	**-525**
Zn(II)	-453,644	-64,642	-972,843	**-573**
Cu(II)	-453,644	-195,081	-1103,356	**-619**
Ni(II)	-453,644	-168,177	-1076,522	**-664**
Pd(II)	-453,644	-125,592	-1033,926	**-656**
Pt(II)	-453,644	-117,978	-1026,349	**-679**

Ha: Hartree and Method: B3LYP/G-311++(d,p)-LANL2DZ (Metal)

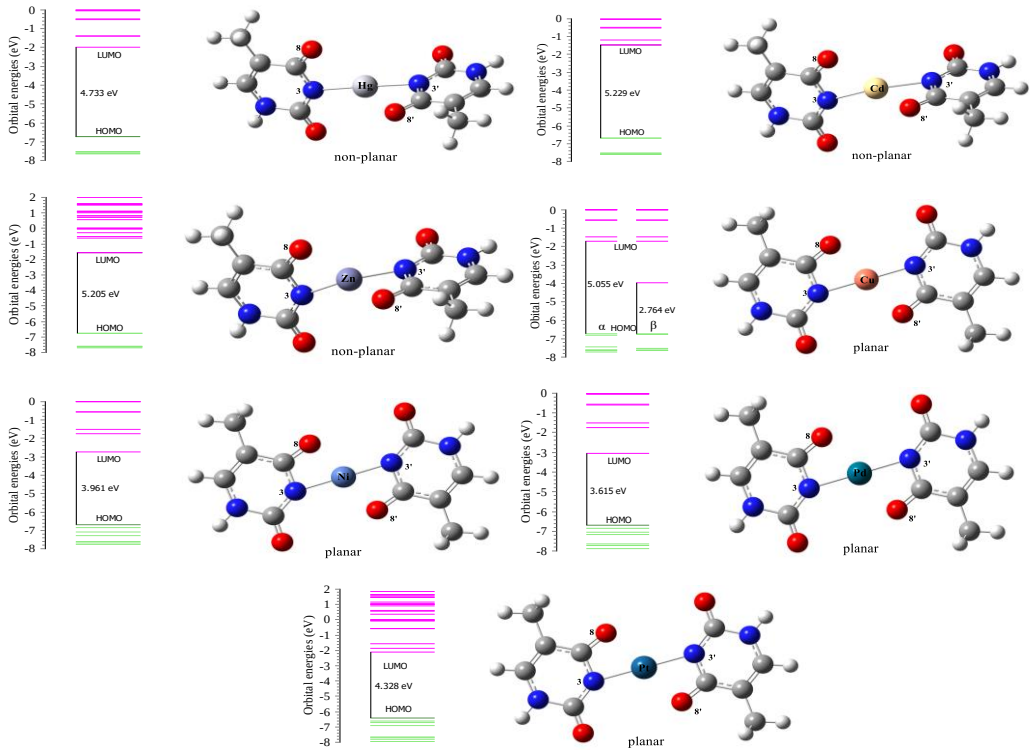

Fig. 6. Optimized metal-mediated thymine complexes and their HOMO-LUMO energy gaps. Atoms are shown in a ball and stick representation with standard colors. (Red=O; White=H; Blue=N; Cyan=C). In the orbital energies, green lines and pink lines represent HOMO (OMOs) and LUMO (UMOs) energy levels, respectively. Also, geometries are determined as planar or non-planar.

Orbital energy levels and Egap values (eV) for open- and closed-shell complexes are shown in Fig. 6. Referring from Fig. 6, the Egap values of complexes except Cu-complex can be seen that is over the insulation threshold 3 eV (as described in Fig. 3). All these metal complexes are included in the insulation class [39]. When the molecular orbital energy level of the Cu^{2+} (d^9 open-shell) complex is seen that the α-SOMO orbital (singly occupied molecular orbital) has lower energy than the β-HOMO orbital. The SOMO is similar the β-LUMO. Hence, it is clear that the lowest excitation occurs between β-HOMO and β-LUMO. In this system, β-HOMO–β-LUMO difference (2.764 eV) is taken into account for the Egap value. Looking at the other planar complexes, Egap values is seen that is over the 3 eV value. Only Cu-complex is included in the semiconductor class [39].

In many studies related to the conductivity, it is said the conductivity occurs via π-way [42-44]. Non-planar molecular orientation can be assumed in a geometrical manner such as described below:

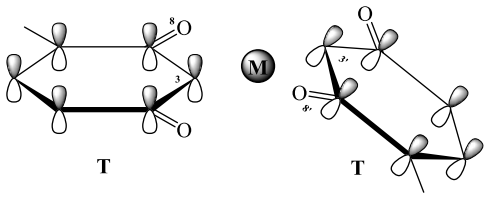

Assumed π-π interaction
at non-planar complexes
(N atoms were hidden)

Referring to this figure, the conjugated π-system of the aromatic thymine ligand is difficult to overlap with the π-system of the ligand on the other side. In other words, π-π interaction is not possible. Therefore, it seems difficult to transmission of electricity through π system in these complexes. Our Egap values are consistent with this explanation. On the other hand, the molecular orientation of planar complexes can be assumed as follows:

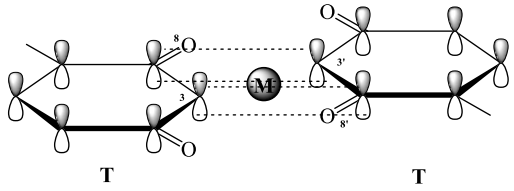

Assumed π-π interaction at planar complexes (N atoms were hidden)

Referring to this orientation, the conjugated π-system of aromatic thymine is easy to overlap with the π-system of the other ligand. In these complexes, the transmission of electricity through π-system can be considered to be occur easily. Our Egap values support this idea. Egap values of planar complexes are lower than those of nonplanar complexes. Even so, Egap values of Ni, Pd ve Pt complexes are over 3 eV. However, these complexes are close to semiconductor class.

According to our calculations, for conductivity applications, most suitable complex is T-Cu-T complex. Among all investigated complexes, best conductor is complex obtained from Cu. This work is expected to lead to nanotechnological applications will be done in the future.

4. Conclusion

In summary, we theoretically design metal-mediated TT base pairs and explore their structure and energy level of the frontier orbitals with a DFT method. On the basis of the obtained results, the following conclusions can be drawn.

In all stable complexes, the metal cation is connected to the side of the deprotonated nitrogen atom (N3) and the oxygen atom at the 2-position of the pyrimidine base.

Our calculations have been carried out without any geometrical constraints. While T-M-T complexes formed from Hg, Cd and Zn metal cations are non-planar, the complexes formed from Cu, Ni, Pd and Pt are planar. It is observed that planarity increases the metal base distance decreases and the planar complexes are more stable than the nonplanar complexes. All the reactions are considerable exothermic and irreversible.

The Egap values of planar complexes are lower than those of nonplanar complexes. Among them, Cu-complex has the lowest Egap value. Thus, this complex is best conductor and it can be used for single nanowires.

Acknowledgments

The numerical calculations reported in this paper were fully/partially performed at TUBITAK ULAKBIM, High Performance and Grid Computing Center (TRUBA resources).

References

[1] L. Berti, G. A. Burley, Nature Nanotechnology 3 (2008) 81-87.

[2] (a) E. Braun, Y. Eichen, U. Sivan, G. Ben-Yoseph, Nature 391 (1998) 775-778. b) J. Richter, M. Mertig, W. Pompe, I. Mnch, H. K. Schackert, Appl. Phys. Lett. 78 (2001) 536-538. c) L. Berti, A. Alessandrini, P. Facci, J. Am. Chem. Soc. 127 (2005) 11216-11217. (d) G. Maubach, D. Born, A. Csa´ki, W. Fritzsche, Small 1 (2005) 619-624.

[3] J. V. Burda, J. Ŝponer, P. Hobza, J. Phys. Chem. 100 (1996) 7250-7255.

[4] J. V. Burda, J. Ŝponer, J. Leszczynski, P. Hobza, J. Phys. Chem. B 101 (1997) 9670-9677.

[5] L. Rulisek, J. Ŝponer, J. Phys. Chem. B 107 (2003) 1913-1923.

[6] M. Noguera, J. Bertran, M. Sodupe, J. Phys. Chem. A 108 (2004) 333-341.

[7] R. Di Felice, A. Calzolari, H. Y. Zhang, Nanotechnology 15 (2004) 1256-1263.

[8] M. Fuentes-Cabrera, B. G. Sumpter, J. E. Ŝponer, J. Ŝponer, L. Petit, J. C. Wells, J. Phys. Chem. B 111 (2007) 870-879.

[9] S. S. Alexandre, J. M. Soler, L. Seijo, F. Zamora, Phys. Rev. B 73 (2006) 205112.

[10] M. Noguera, V. Branchadell, E. Costantino, R. Ríos-Font, M. Sodupe, L. Rodríguez-Santiago, J. Phys. Chem. A 111 (2007) 9823–9829.

[11] Y. Takezawa, M. Shionoya, Acc. Chem. Res. 45 (2012) 2066-2076.

[12] K. Tanaka, M. Shionoya, J. Org. Chem. 64 (1999) 5002-5003.

[13] a) S. S. Mallajosyula, S. K. Pati, Angew. Chem. 121 (2009) 5077-5081 b) G. H. Clever, S. J. Reitmeier, T. Carell, O. Schiemann, Angew. Chem. 122 (2010) 5047-5049.

[14] D. Porath, G. Cuniberti, R. Di Felice, Top. Curr. Chem. 237 (2004) 183-227.

[15] M. Di Ventra, M. Zwolak, American Scientific Publishers 2 (2004) 475-493.

[16] R. G. Endres, D. L. Cox, R. R. P. Singh, Rev. Mod. Phys. 76 (2004) 195-214.

[17] S. S. Mallajosyula, S. K. Pati, J. Phys. Chem. Lett. 1 (2010) 1881-1894.

[18] P. U. Civcir, J. Mol. Struct. 532 (2000) 157-169.

[19] M. Orozco, B. Hernandez, F. Luque, J. Phys. Chem. B 102 (1998) 5228-5233.

[20] Y. Miyake, H. Togashi, M. Tashiro, H. Yamaguchi, S. Oda, M. Kudo, Y. Tanaka, Y. Kondo, R. Sawa, T. Fujimoto, T. Machinami, A. Ono, J. Am. Chem. Soc. 128 (2006) 2172-2173.

[21] Y. Tanaka, S. Oda, H. Yamaguchi, Y. Kondo, C. Kojima and A. Ono, J. Am. Chem. Soc. 129 (2007) 244-245.

[22] Y. Tanaka, H. Yamaguchi, S. Oda, Y. Kondo, M. Nomura, C. Kojima, A. Ono, Nucleosides Nucleotides Nucleic Acids 25 (2006) 613-624.

[23] Y. Tanaka, A. Ono, Dalton Trans. (2008) 4965-4974.

[24] G. H. Clever, C. Kaul, T. Carell, Angew. Chem. 2007, 119, 6340; Angew. Chem. Int. Ed. 46 (2007) 6226-6236.

[25] Lippert, B. Coord. Chem. ReV. 200 (2000) 487-516.

[26] J. Ruiz, J. Lorenzo, L. Sanglas, N. Cutillas, C. Vicente, M. D. Villa, F. X. Avilés, G. López, V. Moreno, J. Pérez, D. Bautista, Inorg. Chem. 45 (2006) 6347-6360.

[27] H. Engelking, B. Krebs, J. Chem. Soc., Dalton Trans. (1996) 2409-2416.

[28] a) J. S. Lee, L. J. P. Latimer, R. S. Reid, Biochem. Cell. Biol. 71 (1993) 162-168. b) P. Aich, S. L. Labiuk, L. W. Tari, L. J. T. Delbaere, W. J. Roesler, K. J. Falk, R. P. Steer, J. S. Lee, J. Mol. Biol. 294 (1999) 477-485.

[29] S. D. Wettig, C. Z. Li, Y. T. Long, H. B. Kraatz, Analytical Sciences 19 (2003) 23-26.

[30] A. Rakitin, P. Aich, C. Papadopoulos, Y. Kobzar, A. S. Vedeneev, J. S. Lee, J. M. Xu, Phys. Rev. Lett. 86 (2001) 3670-3673.

[31] F. Moreno-Herrero, P. Herrero, F. Moreno, J. Colchero, C. Gomez-Navarro, J. Gomez-Herrero, A. M. Baro, Nanotechnology 14 (2003) 128-133.

[32] B. Liu, A. J. Bard, C. Z. Li, H. B. Kraatz, J. Phys. Chem. B 109 (2005) 5193-5198.

[33] G. Brancolini, R. Di Felice, J. Phys. Chem. B 112 (2008) 14281-14290.

[34] G. Brancolini, R. Di Felice, J. Chem. Phys. 134 (2011) 205102.

[35] (a) A. Schaefer, H. Horn, R. Ahlrichs. J. Chem. Phys. 93 (1992) 2571-2577. (b) P. J. Hay, W. R. Wadt, J. Chem. Phys. 82 (1985) 270283. (c) P. J. Hay, W.R. Wadt, J. Chem. Phys. 82 (1985) 284-298. (d) P. J. Hay, W.R. Wadt. J. Chem. Phys. 82 (1985) 299-310.

[36] Gaussian 09, Revision D.01, M. J. Frisch, G. W. Trucks, H. B. Schlegel, G. E. Scuseria, M. A. Robb, J. R. Cheeseman, G. Scalmani, V. Barone, B. Mennucci, G. A. Petersson, H. Nakatsuji, M. Caricato, X. Li, H. P. Hratchian, A. F. Izmaylov, J. Bloino, G. Zheng, J. L. Sonnenberg, M. Hada, M. Ehara, K. Toyota, R. Fukuda, J. Hasegawa, M. Ishida, T. Nakajima, Y. Honda, O. Kitao, H. Nakai, T. Vreven, J. A. Montgomery, Jr., J. E. Peralta, F. Ogliaro, M. Bearpark, J. J. Heyd, E. Brothers, K. N. Kudin, V. N. Staroverov, T. Keith, R. Kobayashi, J. Normand, K. Raghavachari, A. Rendell, J. C. Burant, S. S. Iyengar, J. Tomasi, M. Cossi, N. Rega, J. M. Millam, M. Klene, J. E. Knox, J. B. Cross, V. Bakken, C. Adamo, J. Jaramillo, R. Gomperts, R. E. Stratmann, O. Yazyev, A. J. Austin, R. Cammi, C. Pomelli, J. W. Ochterski, R. L. Martin, K. Morokuma, V. G. Zakrzewski, G. A. Voth, P. Salvador, J. J. Dannenberg, S. Dapprich, A. D. Daniels, O. Farkas, J. B. Foresman, J. V. Ortiz, J. Cioslowski, and D. J. Fox, Gaussian, Inc., Wallingford CT, 2010.

[37] R. Dennington, T. Keith, J. Millam, GaussView, Version 5, Semichem Inc., Shawnee Mission, KS, 2009.

[38] L. V. Skripnikov, Chemissian V. 4.43, Visualization Computer Program, www.chemissian.com, 2016.

[39] M. M. Kerileng, M. N. Peter, F. A. Rachel, M. Gcineka, M. M. Stephen, N. Njagi, M. Milua, B. Priscilla, I. I. Emmanuel, Int. J. Electrochem. Sci. 7 (2012) 11859-11875.

[40] Y. Cheng, S. H. Yang, C. Hsu, Chem. Rev. 109 (2009) 5868-5923.

[41] A. Rakitin, P. Aich, C. Papadopoulos, Y. Kobzar, A. S.Vedeneev, J. S. Lee, J. M. Xu, Physical Review Letters 86 (2001) 3670-3673.

[42] P. J. Dandliker, R. E. Holmin, J. K. Barton, Science 275 (1997) 1465-1468.

[43] D. B. Hall, R. E. Holmin, J. K. Barton, Nature 382 (1996) 731-735.

[44] M. R. Arkin, E. D. A. Stemp, R. E. Holmlin, J. K. Barton, A. Hörmann, E. J. C. Olson, P. F. Barbara, et al., Science 273 (1996) 475-780.